PENSOFT
SENCKENBERG world of biodiversity
Leibniz Association

How the youngsters teach the "old timers": Terminology of turbinals in adult primates inferred from ontogenetic stages

Franziska Wagner[1,2], Valerie Burke DeLeon[1], Christopher J. Bonar[3], Timothy D. Smith[2]

1 *Department of Anthropology, University of Florida, 330 Newell Dr, Gainesville, FL 32611, USA*
2 *School of Physical Therapy, Slippery Rock University, 108 Central Loop, Slippery Rock, PA 16057, USA*
3 *Franklin Park Zoo, One Franklin Park Road, Boston, MA 02121, USA*

https://zoobank.org/BAD3E8A8-116E-4FDF-A4EE-D2F296400DA5

Corresponding author: Franziska Wagner (franziska.wagner@sru.edu)

Academic editor Clara Stefen | **Received** 7 May 2024 | **Accepted** 6 August 2024 | **Published** 23 August 2024

Citation: Wagner F, DeLeon VB, Bonar CJ, Smith TD (2024) How the youngsters teach the "old timers": Terminology of turbinals in adult primates inferred from ontogenetic stages. Vertebrate Zoology 74 487–509. https://doi.org/10.3897/vz.74.e126944

Abstract

Comparative studies rely on the identification of homologous traits, which is challenging especially when adult stages alone are available. Inferring homology from developmental series represents the most reliable approach to recognize similar phenotypes. The primate nasal cavity exhibits a plastic morphology (shape) and topology (structure) which challenge the terminology of turbinals. Turbinal development largely corresponds to the therian template: turbinals emerge from the cartilaginous nasal capsule, ossify endochondrally, and increase their size through appositional bone growth. We studied histological serial sections and µCT data of eleven primate species in six genera representing four to five age stages (fetal to adult), and the neonate and adult stage of another primate species. We reconstructed cartilaginous precursors and followed their growth patterns until adulthood to inform the identification of structures. The developmental stages were transformed to character states for better comparison across the sample. Strepsirrhines conserved the plesiomorphic condition, with turbinal morphology similar to other placentals. In contrast, haplorhines showed a reduced turbinal number. Most strikingly, some cartilaginous turbinals are absent in the ossified nasal cavity (*Saguinus*); others seem to emerge as appositional bone without a cartilaginous precursor (*Aotus*, *Pithecia*). Our observation that successive developmental sequences differ from the established placental template emphasizes the significance of ontogenetic series for comparative anatomy. Structures which exhibit analogous growth patterns might be falsely considered as being homologous in adults, resulting in biased phenotypic data that strongly affects comparative analyses (e.g., phylogenetic reconstructions).

Keywords

Chondrification, haplorhines, histology, morphology, nasal concha, ossification, strepsirrhines, turbinate

Introduction

The identification of homologous phenotypic traits among species is a prerequisite in comparative studies (Haszprunar 1998, Sereno 2007; McCune and Schimenti 2012). Nevertheless, phenotypic data may be inaccessible due to missing data (research gaps), ambiguous terminologies, or restricted availability of both raw and derived data (Stefen et al. 2022; Christmas et al. 2023). This can be observed, e.g., in the morphology of the mammalian

nasal cavity. In the last century research on intracranial morphology was limited by destructive methods required to obtain the nasal cavity (e.g., Paulli 1900a, 1900b, 1900c). Though the establishment of modern imaging techniques like high-resolution computed tomography (μCT) increased the number of investigated species, the scanning costs continue to keep it constrained (Van Valkenburgh et al. 2014). Second, various terminologies for internal nasal structures are used in literature (e.g., Allen 1882; Seydel 1891; Voit 1909), resulting in ambiguous homologies of individual ethmoidal turbinals across mammals (i.e., ethmoturbinals, frontoturbinals, and interturbinals, which are thin bony lamellae attached to the lateral nasal wall, hereafter called turbinals). The most established approach to identify and homologize turbinals is closely associated with ontogenetic patterns, like the relative point in time at which the individual structures develop (Reinbach 1952a, 1952b; Zeller 1983, 1989; Macrini 2012, 2014). Growth patterns of the pre- and early postnatal nasal capsule serve as the most reliable source of information to explain homology. Therefore, investigations of turbinal morphology in adults require comparative ontogenetic series (Maier 1993a; Macrini 2014; Maier and Ruf 2014; Ito et al. 2021, 2022). Since the sampling of suitable prenatal stages is challenging – especially for viviparous model organisms like placentals (e.g., domestic dog, Bonnet 1897) – such comprehensive developmental series are available for a restricted number of species (Semon 1894; Werneburg et al. 2013; Werneburg and Yaryhin 2018).

Primates are recognized by their modified turbinal morphology due to a developmental tradeoff between the nasal capsule and surrounding structures (encroaching orbit, reduced olfactory bulb size, shifted frontal lobes) (Maier 1993b; Smith and Rossie 2006; Smith et al. 2014a, 2021b). The reduced number and simplified shape of the turbinals, especially in haplorhines, challenges their identification based on patterns observed in a vast number of species across mammalian orders (e.g., *Oryctolagus*, Voit 1909; *Dasypus*, Reinbach 1952a, 1952b; *Tupaia*, Zeller 1983; *Monodelphis*, Macrini 2014): In the case of elements that develop in a serially homologous fashion (e.g., teeth, digits, or turbinals) it can be uncertain which element is lost in cases where fewer than the full (plesiomorphic) number of structures appear in the adults (e.g., Swindler 2002; Macrini 2012; Kavanagh et al. 2020). Moreover, assuming serial homology of turbinals is sometimes problematic (Macrini et al. 2023), perhaps especially because developmental studies have identified cases of turbinal loss (e.g., Ito et al. 2021). Here, we make few assumptions of turbinal homology, except those that appear to broadly characterize all therian mammals (placentals and marsupials). In particular, all therians exhibit a similar grundplan, or template, in the form of a tripartite cartilaginous nasal capsule (Maier 1993a; Macrini 2012). This organization, explained more fully below, aids in identification of types of turbinals of the ethmoid bone (i.e., ethmoturbinals I to IV, frontoturbinals, and interturbinals), although it cannot resolve the issue of identity of serial subtypes (e.g., ethmoturbinal II, III, etc.).

Aim of the study

The overall goal of the present study is the identification of turbinals and associated structures (e.g., semicircular crest) among three primate lineages based on the observed developmental patterns of the mammalian nasal capsule. Because we are studying relatively rare and slowly reproducing species, our sample size is small; our results admittedly will suffer from the lack of a broad phylogenetic foundation, the same deficit that may be attributed to old literature on the chondrocranium (see further discussion of this point by Sánchez-Villagra and Forasiepi 2017). However, numerous studies have relied on samples with developmental stages to establish the identity of, or to infer the absence of, individual turbinals (e.g., Macrini 2012; Ito et al. 2021; Macrini et al. 2023). Identification of developmental patterns can, in turn, provide critical evidence for broader phylogenetic analyses (Macrini et al. 2023). Whereas establishing the precise homology of turbinals is beyond the scope of the present study, our developmental data provide critical context for the turbinal anatomy of adult primates, recently comprehensively studied by Lundeen and Kirk (2019) and Lundeen and Kay (2022), and will broaden our knowledge of comparative nasal development of primates, which is currently restricted mainly to a small number of strepsirrhines (Smith et al. 2007; Smith and Rossie 2008).

Ultimately, our study will also support future efforts to record traits as numeric codes across a large species sample (phenotyping approach by Sereno 2007; Stefen et al. 2022). The coding of descriptive (i.e., text-based) phenotypic traits makes them computer-parsable and accessible to analyzing software for genotype-phenotype alignments and phylogenetic analyses (Stößel et al. 2010; Stefen et al. 2022; Christmas et al. 2023). Previous studies correlated genomic data (e.g., number of olfactory receptor genes, OR genes) with continuous morphometric data like turbinal surface area measurements (e.g., Martinez et al. 2023, 2024a).

Methods

Sample

The present study is part of a project which aims to associate phenotypic traits of the nasal cavity in primates with their sequenced OR gene data. Therefore, the selection of primate species was based on two preconditions: the availability of a fully sequenced genome, followed by the access to image data for comprehensive age stages. Genome data are available for 45 primate species so far; OR gene data have been extracted for 43 species (Zoonomia Consortium: Genereux et al. 2020; Christmas et al. 2023). The phylogenetic relationships among the sampled species were adapted from the Zoonomia Consortium (https://zoonomiaproject.org/the-mammal-tree-view; Genereux et al. 2020) (Fig. 1).

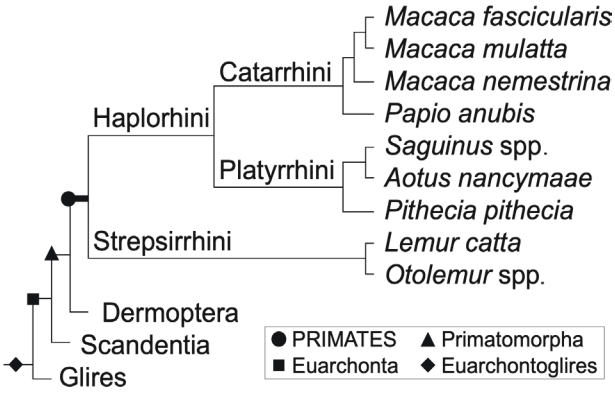

Figure 1. Topology of the placental grandorder Euarchontoglires, that was adapted from the Zoonomia Project (https://zoonomiaproject.org/the-mammal-tree-view). The seven selected primate genera cover the higher lineages Haplorhini: Catarrhini (n = 2), Haplorhini: Platyrrhini (n = 3), and Strepsirrhini (n = 2). Glires includes Rodentia and Lagomorpha.

Obtaining a comprehensive intraspecific ontogenetic series of imaging data is challenging—especially when the sample selection was further limited by access to genomic data. Because we expect little variation between closely related species (e.g., Paulli 1900c), some of our age series were selected on genus level (i.e., sister species with unknown OR gene data) to increase the age range. For instance, we included an age series of tamarins that are especially closely related, the bare-faced tamarin group (*Saguinus oedipus* and *S. geoffroyi*, Rylands et al. 2016). Other species are selected for ontogenetic information on adult primates previously studied by other authors (e.g., Lundeen and Kirk 2019). In total, our current sample of imaging data included seven primate genera, for all of which OR gene data are available. Six of them cover four to five ontogenetic stages (fetal to adult; as inferred from exact age or laboratory notes like "late fetal", see below and Table 1). They equally represent three higher taxa (1) Strepsirrhini (*Lemur* and *Otolemur*), (2) Haplorhini: Platyrrhini (*Aotus* and *Saguinus*), (3) Haplorhini: Catarrhini (*Papio* and *Macaca*) (Table 1, Fig. 1). One caveat is that similar life stages (e.g., "neonate") are nevertheless at different points of development (heterochrony; Smith et al. 2016; Werneburg and Yaryhin 2018). The turbinal growth in each of the six ontogenetic series serves to identify possible lineage-specific patterns. A third platyrrhine, *Pithecia*, is represented by a neonate and an adult stage.

The selection of fetal and perinatal specimens was intended to provide novel information on the grundplan of the primate nasal capsule, in combination with prior observations (e.g., Maier 1980, 2000; Smith and Rossie 2008; Maier and Ruf 2014). Thirty cadaveric specimens were used to create anatomic reconstructions (Table 1). No specimens were sacrificed for this study. All fetal or newborn specimens and some juveniles and adults died of natural causes in captivity at zoos or primate research centers. Subadult and adolescent *M. nemestrina* were acquired from a laboratory conducting research unrelated to our study, after the animals were sacrificed (see Smith et al. 2001). For some specimens the exact age or at least the age stage (neonate, juvenile, etc.) was noted. For instance, the late fetal *P. anubis* Papio107 died at 150 days gestation (average total gestation length 180 days, Smuts and Nicolson 1989). Commonly, adult mammals are recognized by their fully erupted permanent dentition (Smith et al. 2020). However, in the *M. nemestrina* A3 (female, 4 years, 4 months, and 20 days) all M2/m2 are in occlusion, whereas no M3/m3 has yet erupted. Sexual maturity is reached at about 35 months in females (see table 1 in Harvey and Clutton-Brock 1985). Thus, this specimen was certainly sexually mature, although dentally it was not fully adult. Some skeletonized specimens were acquired for scanning directly from museums (or indirectly from MorphoSource, https://www.morphosource.org, for the for the Media ID see Table 1). Some specimens were prepared for histological study in prior studies (as cited in Table 1). Except for skeletonized museum specimens, all cadaveric specimens were stored in 10% buffered formalin prior to scanning and/or histology. Some specimens were frozen first prior to formalin immersion; these were excluded from histological methods.

CT scanning, histological preparation, and virtual 3D reconstruction

Whole heads and bodies, respectively, have been scanned with the GE V|TOME|X M 240 nano-CT device housed at the Nanoscale Research Facility, University of Florida, Gainesville. Additional µCT data used in previous studies and stored in the laboratories of VBD/TDS were included, along with image volumes obtained from the database MorphoSource (Table 1). The resolution (cubic voxel size) of the scans ranged from 0.020500 to 0.093786 mm.

Some histological material has been investigated in previous studies (Table 1). The preparation of each specimen (here on the example of Aotus1) at the School of Physical Therapy, Slippery Rock University followed the protocol described in DeLeon and Smith (2014). After CT scanning, the specimen was restored to 10% neutral buffered formalin. The right hemiface (septum included) was trimmed with a scalpel from the nose tip up to the caudal end of the olfactory recess as inferred from the CT scans. Most of the soft tissues surrounding the nasal cavity (eye, skin, muscles, etc.) were removed and the zygomatic was cut. For the decalcification, 50 g sodium citrate ($C_6H_5Na_3O_7$) was dissolved in 125 ml formic acid (CH_2O_2) and diluted to 500 ml with distilled water (Evans and Krajian 1930). The solution was replaced weekly and simultaneously the progress of decalcification was tested by mixing 5 ml of the solution taken from the bottom of the jar with 1 ml of a sodium/aluminum oxalate solution (5 g sodium oxalate $Na_2C_2O_4$ dissolved in 100 ml distilled water, lightly boiled and cooled). After the decalcification was complete (sodium oxalate no longer precipitates), the specimen was stored in fresh decalcifier for one additional week and returned to 10% neutral buffered formalin. Prior to paraffin embedding, the specimen was dehydrated by a gradual series of ethanol concentrations (50%

Table 1. List of primate specimens whose ethmoidal region has been investigated in the current study. The list covers seven genera of three major lineages Haplorhini: Strepsirrhini (n = 2), Haplorhini: Platyrrhini (n = 3), and Haplorhini: Catarrhini (n = 2). Six genera cover at least four age stages (fetal to adult). As the developmental and morphological patterns of the ethmoidal region are similar between closely related species, some age stages of a genus cover more than one species. The specimens and the CT scans originated from different labs (origin); the data were completed by surveys of the online data repository MorphoSource (MS, https://www.morphosource.org/). The descriptive analyses are based on histological serial sections (stained alternately with Gill's Hematoxylin-Eosin and Gomori-Trichrome; thickness of sections given) and/or µCT/diceCT data (given are cubic voxel size, voltage, and current of the scan). Some specimens have been used in previous studies. For some individuals, detailed information on their age and sex was provided.

Species	Specimen ID	Stage (age)	Origin specimen (S); CT data (CT)	Histology Section thickness (mm)	µCT (u) / diceCT (d)			Used in study	Notes
					Voxel size (mm^3)	Voltage (kV)	Current (µA)		
Strepsirrhini									
Lemur catta	DLC 6888	Fetal (12–18D premature)	DLC^{S}	0.010	NA	NA	NA	Smith et al. (2016)	
L. catta	DLC 6834	Neonate (5D)	DLC^{S}	0.010	–	–	–	Smith et al. (2016)	Male
L. catta	DLC 6938f	Early infant	DLC^{S}; CJV^{CT}	–	0.020500^{u}	70^{u}	114^{u}	Wood et al. (2023)	Female
L. catta	LCD 100121	Juvenile	KP^{S}; CJV^{CT}	–	0.030000^{u}	70^{u}	114^{u}	Wood et al. (2023)	Male
L. catta	CMZ 930402 (aka Lc2)	Adult (15Y, 5M, 16D)	CMZ^{S}; CJV^{CT}	–	0.035000^{u}	70^{u}	114^{u}	Smith et al. (2016)	Female
Otolemur crassicaudatus	DLC 2810	Late fetal	DLC^{S}	0.010	–	–	–	Smith et al. (2017)	
O. crassicaudatus	DLC 2824	Neonate (6D)	DLC^{S}	0.010	–	–	–	Smith et al. (2017)	Female
O. crassicaudatus monterri	DLC 2728	Infant (86D)	DLC^{S}; CJV^{CT}	–	0.025000^{u}	70^{u}	114^{u}	Wood et al. (2023)	
O. garnettii	CMNH-B0748	Adult	$CMNH^{s}$; CJV^{CT}	–	0.030000^{u}	70^{u}	114^{u}	NA	
Haplorrhini: Platyrrhini									
Aotus nancymaae	Aotus108	Neonate	MK^{S}; CJV^{CT} NEOMED	0.010	0.030000^{u}	70^{u}	114^{u}	Smith et al. (2023)	Stillborn, male
A. nancymaae	Aotus101	Neonate	DC^{S}	0.010	–	–	–	Smith et al. (2015)	Stillborn
A. nancymaae	Aotus104	Infant (14D)	DC^{S}; CJV^{CT}	0.010	0.039000^{u}	70^{u}	114^{u}	Smith et al. (2023)	
A. nancymaae	Aotus107	Juvenile (3M)	DC^{S}; CJV^{CT}	–	0.020500^{u}	70^{u}	114^{u}	Smith et al. (2023)	
A. nancymaae	Aotus102	Subadult	DC^{S}; CJV^{CT}	–	0.020500^{u}	70^{u}	114^{u}	Smith et al. (2023)	
A. nancymaae	Aotus1	Adult	DWA^{S}; CJV^{CT}	0.012	0.035000^{u}	70^{u}	114^{u}	Smith et al. (2023)	
Saguinus geoffroyi	SG10 (MM0321)	Mid-fetal	CMZ^{S}	0.010	–	–	–	Smith et al. (2008)	Aborted
S. geoffroyi	SG3 (MM0880)	Neonate (0D)	CMZ^{S}	0.010	–	–	–	Smith et al. (2008)	Female
S. geoffroyi	MM105	Infant (1M, 23D)	CMZ^{S}	0.010	–	–	–	Smith et al. (2008)	Male
S. midas	Smidas (8452)	Juvenile (5M)	TX^{S}	0.010	–	–	–	Smith et al. (2008)	Male
S. geoffroyi	CJV80-Sgo408-88	Adult	$NEPC^{S}$; CJV^{CT}	–	0.025000^{u}	70^{u}	114^{u}	NA	
S. imperator	M60903	Adult (11Y, 4M, 15D)	CMZ^{S}; CJV^{CT}	–	0.030000^{u}	70^{u}	114^{u}	NA	Female
S. oedipus	So2 (Sg0-83)	Adult (3.5Y)	$NEPC^{S}$	0.010	–	–	–	Smith et al. (2008)	Male
Pithecia pithecia	Saki2	Neonate	CMZ^{S}	0.010	–	–	–	Smith et al. (2023)	
P. pithecia	Saki3 (CMZ 160705)	Neonate (0D)	CMZ^{S}; VBD^{CT}	0.010	0.0319683^{d}	120^{d}	300^{d}	NA	Female, stillborn
P. pithecia	CMNH-11-F3	Adult	$CMNH^{S}$; CJV^{CT}	–	0.039000^{u}	70^{u}	114^{u}	NA	Female

Species	Specimen ID	Stage (age)	Origin specimen (S); CT data (CT)	Histology Section thickness (mm)	µCT (u) / diceCT (d)			Used in study	Notes
					Voxel size (mm^3)	Voltage (kV)	Current (µA)		
Haplorrhini: Catarrhini									
Macaca fascicularis	NA	Fetal	Maier (2000)	NA	–	–	–	Maier (2000)	CRL 55 mm
M. mulatta	YN09-175	Neonate	YRPC^{S}	0.010	–	–	–	Smith et al. (2015)	
M. fascicularis	mcz:mamm:23812	Adult	MCZ^{S}; MS^{CT} (Media ID 000003030)	–	0.061559^{u}	NA	NA	NA	Male
M. mulatta	MCZ:Mamm:26475	Adult	MCZ^{S}; MS^{CT} (Media ID 000003052)	–	0.090751^{u}	NA	NA	NA	
M. nemestrina	516-A6	Subadult	NYU^{S}; CJV^{CT} NEOMED	–	0.035000^{u}	70^{u}	114^{u}	This study	
M. nemestrina	A3	Adolescent (4Y, 4M, 20D)	NYU^{S}; VBD^{CT} NRF	–	0.079556^{u}	140^{u}	260^{u}	This study	Body weight at death 4,400 g
Papio anubis	NA	Fetal	Maier (2000)	NA	–	–	–	Maier (2000)	CRL 115 mm
P. anubis	Papio107 (40206)	Late fetal (150D gestation)	YRPC^{S}; CJV^{CT} NEOMED	–	0.035000^{u}	NA	NA	This study	
P. anubis	Papio108(38821)	Older infant (1Y, 32D)	YRPC^{S}; VBD^{CT} NRF	–	0.078851^{u}	140^{u}	280^{u}	This study	
P. anubis	amnh:mammals: m-51380	Adult	AMNH^{S}; MS^{CT} (Media ID 000016131)	–	0.093786^{u}	NA	NA	NA	

–, no data; **NA**, information not available; CRL, crown-rump length; **Ages**: D, day/s; M, month/s; Y, year/s; **Sources**: **AMNH**, American Museum of Natural History; **CJV**, specimen scanned by Christopher J. Vinyard (Northeast Ohio Medical University); **CMNH**, Cleveland Museum of Natural History; **CMZ**, Cleveland Metroparks Zoo; **DC**, Dumond Conservancy; **DLC**, Duke Lemur Center; **DWA**, Dallas World Aquarium; **MCZ**, Museum of Comparative Zoology, **MK**, Michale E. Keeling Center for Comparative Medicine and Research; **NEPC**, New England Primate Research Center; **TX**, Gladys Porter Zoo; **VBD**, lab of Valerie B. DeLeon (University of Florida); **YRPC**, Yerkes Regional Primate Research Center. **Scan locations**: **NEOMED**, Northeast Ohio Medical University; **NRF**, Nanoscale Research Facility, University of Florida.

up to 100%), cleared in xylene for about 3 hours, and transferred to melted paraffin. The block was placed in a vacuum oven (at 60°C) to enable the paraffin to penetrate the tissue and replace the air. After the paraffin had completely hardened, Aotus1 was sectioned at 12 µm with a rotary microtome. The previously obtained histological specimens were sectioned at 10 or 12 µm (Table 1). Every 5th section was mounted on a glass slide and selected sections were stained either with Gill's Hematoxylin-Eosin or with Gomori-Trichrome (Gomori 1950; Gill et al. 1974).

We used 3D Slicer software (version 5.4.0 to 5.6.0; https://www.slicer.org, Fedorov et al. 2012) to reconstruct the CT data volumes. First, for better comparison between histology and CT, each volume was transformed to match the coronal view. Afterwards, the resampled TIFF image stacks were reconstructed to virtual 3D models by extracting bone surfaces in the Segment Editor tool. The histological sections were examined with a Leica DMLB photomicroscope connected to an AxioCam NRc5 Firewire digital camera, and with a Zeiss stereo microscope connected to an AxioCam 105 color Firewire digital camera. Photographed sections were exported as JPEG image files. The availability of histological serial sections in addition to the CT scans provided detailed information on soft tissues and especially the cartilage in some preadult specimens. The CT scans in turn facilitated the comparative examination of the overall shape of the developing turbinal skeleton within the nasal cavity based on the reconstructed virtual 3D models.

Terminology

The terminology of the turbinals follows the scheme used, e.g., by Voit (1909), Reinbach (1952a, 1952b), and Maier (1993a, 1993b). Turbinals emerge on the nasal side wall (paries nasi) of the cartilaginous nasal capsule and are identified according to ontogenetic patterns which refer to the common template observed in placentals and marsupials. (1) The tripartite nasal capsule is divided into the pars anterior (housing the maxilloturbinal and the nasoturbinal), the pars posterior (housing ethmoturbinals, ETs, and interturbinals, ITs), and the pars lateralis (pars intermedia; housing frontoturbinals, FTs, and ITs) (Voit 1909; Reinbach 1952a; Smith and Rossie 2008). (2) Both ETs and FTs exhibit a species-specific number and are enumerated from rostral to caudal, starting with ET I and FT 1, respectively (Paulli 1900a, 1900b, 1900c; Macrini 2012; Ruf 2014; Wagner and Ruf 2021) (3) The ITs develop at later stages and seldom achieve the size and medial expansion like the enclosing ETs and FTs (Reinbach 1952a, 1952b; Zeller 1983; Smith and Rossie 2008). The presence of ITs varies within a species, and individually between the left and the right nasal fossa (Ruf 2014; Wagner and Ruf 2019, 2021). The IT between ET I and II is most prominent, and, in association with three ETs, regarded as part of the placental template (Schrenk 1989; Ruf 2014). (4) We follow the scheme of Reinbach (1952a, 1952b) and other authors that ET I is rostrally separated into two laminae, lamina anterior (LA) and lamina posterior (LP), since both fuse to each other and continue caudally into the cribriform plate as a uniform turbinal. Each of them elongates rostrally and forms an anterior process (Reinbach 1952a, 1952b; Wagner and Ruf 2021). If no caudally positioned lamina merges with the LA, the LP was considered as being absent. (5) In several placental groups including primates, the semicircular crest (LS) forms an uncinate process (PU) (Maier and Ruf 2014; Paulli 1900a, 1900b, 1900c).

In-text abbreviations: ET, ethmoturbinal; **FT**, frontoturbinal; **IT**, interturbinal; **LA**, lamina anterior (of ET I); **LP**, lamina posterior (of ET I); **LS**, lamina semicircularis; **PU**, processus uncinatus.

Recording of ontogenetic stages

The raw data for the intranasal development were collected descriptively. To compare the growth patterns between individual morphological structures and across the age series, we transformed the text-based ontogenetic stages to distinct character states according to Sereno's (2007) approach of trait recording ("phenotyping"). The definition of seven ontogenetic character states was adapted from developmental mechanisms described by, e.g., Smith et al. (2021a) (Table 2). For each specimen, the developmental stage for each structure (ETs, FTs, IT, LS, PU) was assigned one of the seven character states. The results were illustrated in schemes.

Results

Comparative developmental morphology

Strepsirrhini

Lemur catta

In the earliest stage, a late fetal *L. catta* (DLC 6888; age 12 to 18 days prior to term), the entire nasal capsule, including all turbinals, remains cartilaginous (Fig. 2A–E). Chondrification appears complete throughout the nasal capsule; no regions of mesenchymal tissue are apparent in any parts of the capsule. The pars posterior houses four ETs and an IT between ET I and II. ET I is divided into the LA and LP (Fig. 2A–E). The leading edge of the LA is thimble-shaped, with a posteriorly oriented cavity. There are three FTs within the pars lateralis which are simpler in morphology compared to the neonate (see below). The most rostral one next to the LS is curled dorsally, the intermediate FT and the most caudal FT next to ET I point ventrally (Fig. 2B). The LS and PU are entirely cartilaginous.

Table 2. Coding of ontogenetic stages of the ethmoidal region across the age series in primates according to the phenotyping approach adapted from Sereno (2007). The trait (called locator in Sereno 2007) Ontogeny and its assigned variable Stage was assigned seven distinct character states which refer to the developmental stages mainly according to Smith et al. (2021a). All three so-called minimum standards (sensu Sereno 2007) are defined by using an ontology (Ontology Lookup Service, including the UBERON ID, https://www.ebi.ac.uk/ols4/index) and references, respectively. For all age stages across the sample each structure (turbinals, semicircular crest, uncinate process) was assigned one state. The recording is illustrated in schemes (Figs S15, S16).

Minimum standard	**Definition**
Locator – Ontogeny	"The process of individual development from a single cell, an egg cell or a zygote, to an adult organism is known as ontogeny." (Cabej 2012: 307); "the development of vertebrate embryos proceeds from general features, which are shared by all of them, to more specific features" (Cabej 2012: 310).
Variable – Stage	"Stage defines … a period of time. The word stage is explained as 'one of the distinguishable periods of growth and development of a plant or animal' (Merriam Webster)." (Cabej 2012: 310); "[a] spatiotemporal region encompassing some part of the life cycle of an organism" (UBERON:0000105); the stages and their definitions refer to the development of the turbinal skeleton.
Character states	
– Epithelial bulge	Based on fissuration, the "[f]ormation of clefts into the nasal wall that result in projecting contours" (Smith et al. 2021a: 895).
– Mesenchymal condensation	Process by which "… a simple mass with well-vascularized dispersed mesenchyme … condenses" (Smith et al. 2021a: 888).
– Mesenchyme	"Portion of tissue composed of mesenchymal cells (motile cells that develop from epithelia via an epithelial to mesenchymal transition) and surrounding extracellular material. … In vertebrates, it derives largely from mesoderm, and sometimes the terms are used interchangeably, e.g., lateral plate mesoderm/mesenchyme" (UBERON:0003104).
– Chondrification	"Cell condensation that is an aggregation of mesenchymal cells that are committed to differentiate into chondroblasts and chondrocytes" (UBERON:0005863; synonym Cartilaginous condensation).
– Cartilage	"Skeletal tissue that is avascular, rich in glycosaminoglycans (GAGs) and typically includes chondrocytes within isolated lacunae. Cartilage tissue is deposited by chondroblasts" (UBERON:0002418).
– Endochondral ossification	"Replacement ossification wherein bone tissue replaces cartilage" (UBERON:GO:0001958).
– Bone	"Skeletal tissue with a collagen-rich extracellular matrix vascularized, mineralized with hydroxyapatite and typically including osteocytes located in lacunae that communicate with one another by cell processes (in canaliculi). Bone is deposited by osteoblasts." (UBERON:0002481). Entire cartilaginous tissue has fully ossified; no cartilage remains (own definition F. Wagner).

In a neonatal specimen (DLC 6834, Fig. 2F–H), ossification of the LA and LP of ET I has commenced (Fig. 2F, G), whereas all more posterior turbinals (ET II to IV, IT between ET I and II, FT 1 to 3) remain entirely cartilaginous (Fig. 2H, F). The leading edge of the LA of ET I is fully ossified, and the cone shape is now elongated, such that the posteriorly oriented central cavity is larger. The three FTs are now larger, with more complex morphology; the one next to ET I has a ventral and a dorsal lamella (i.e., double scroll; Fig. 2F, H). The LS and PU are nearly completely ossified, with only a small remnant of cartilage remaining.

In an early infant (DLC 6938f), the ossification of all turbinals (ET, FT, IT) and the LS is proceeding in an antero-posterior sequence (Fig. S1). The PU has ossified similarly to the rostral part of the LS (Fig. S1B). The µCT scans reveal that in ET I the anterior process of the LA has fully ossified, whereas in the caudal direction it continues into cartilaginous tissue. In contrast, the LP of ETI has not yet started its rostral elongation (Fig. S1A). Ossification occurs from the distal free margin to the root, as also observed in ET II and the IT between ET I and II. ET II exhibits a bony fusion to the horizontal lamina, which is also ossified, but the later-developed and smaller IT positioned caudal to ET II has ossified only on its most distal edge (Fig. S1D). Proximally, the IT continues into cartilaginous tissue and its root is expected to attach to the cartilaginous part of the horizontal lamina. Note that cartilage is not displayed in µCT scans, but the pattern is inferred from histology in other specimens (Fig. 2H). Similar to the turbinals, the horizontal lamina has started to ossify on its most distal, rostral end, whereas towards the fusion to the dermal bones it remains cartilaginous at this stage (Fig. S1C, D). ET III is at the earliest stage of ossification within the pars posterior; only a small part is displayed in the µCT scan (Fig. S1E). Within the pars lateralis, the most rostral FT 2 has proceeded the furthest in development, FT 3 ventral to it has a smaller ossification center, and FT 1 dorsal to FT 2 is recognized by a small bony tip (Fig. S1A).

In the juvenile *L. catta* (LCD 100121), the entire turbinal skeleton and the LS including the PU have ossified, i.e., in the µCT scan no "gaps" which would indicate the presence of cartilaginous tissue are apparent in the lamellae of the turbinals (Fig. S2). Instead, the turbinals are attached to the horizontal lamina or to the enclosing dermal bones along almost their entire length and are caudally fused to the ossified cribriform plate (Fig. S2C). Compared to the infant, the anterior process of the LA of ET I has continued its rostral growth into the pars anterior. On the other hand, the LP of ET I remains as a shortened lamina without a rostral process (Fig. S2A). In cross-sectional view, only the LA of ET I has become more complex to form a double scroll, whereas the LP of ET I and the more caudal ETs form simpler single scrolls. The three FTs form double scrolls, too (Fig. S2C). ET II

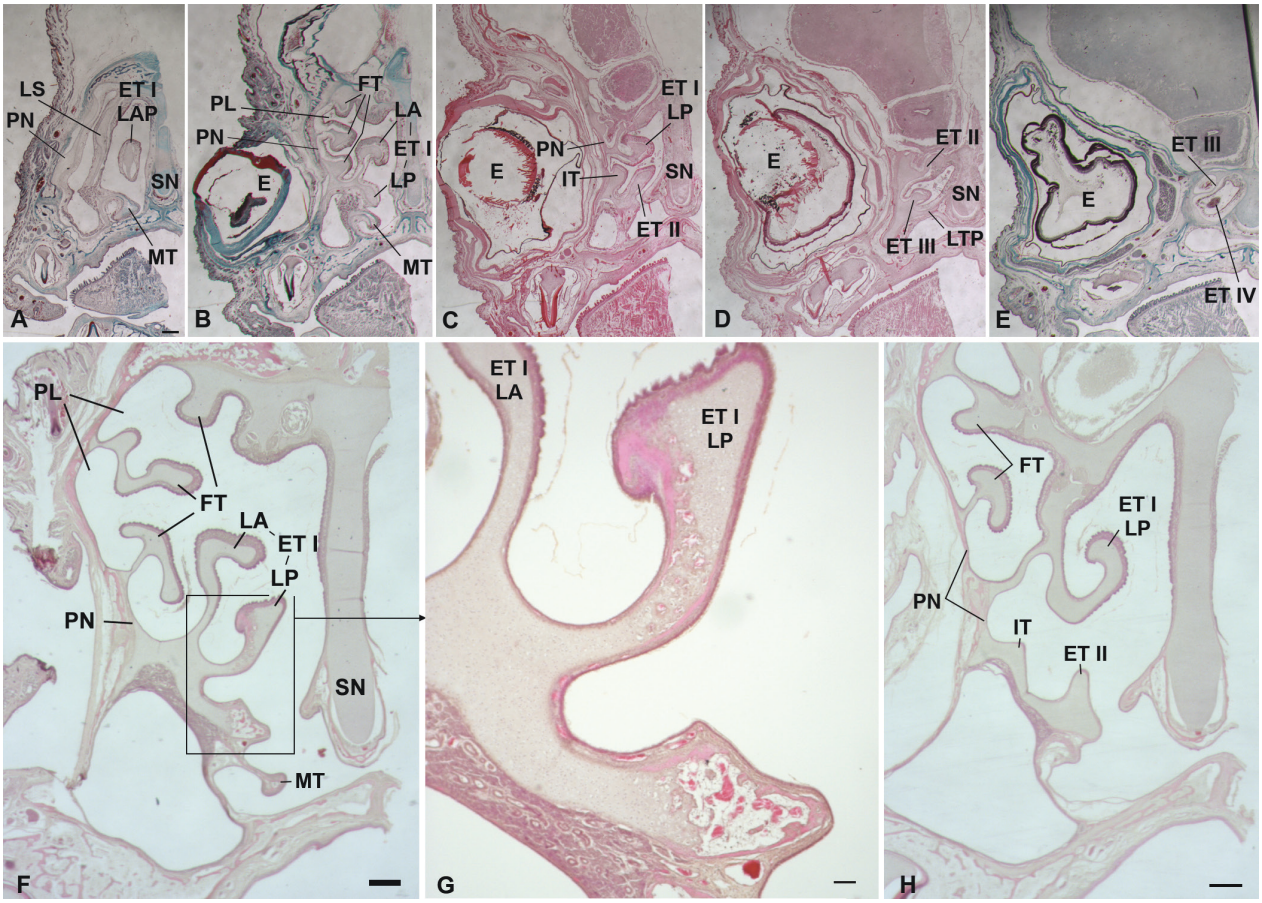

Figure 2. Histology series of two *Lemur catta* stages in coronal plane (rostral to caudal). **A**–**E** Mid to late fetal (DLC 6888). The entire nasal capsule is cartilaginous; **F**–**H** newborn (DLC 6834). **A** Most anterior projection of the anterior lamina (LA) of ethmoturbinal I (ET I), and the semicircular crest (LS) are shown; the maxilloturbinal (MT) is most ventral. **B** ET I has a LA and posterior lamina (LP) at this level. The pars lateralis (PL) is also shown, with three frontoturbinals (FT) within it. **C** At this level the LP begins to attach to the roof of the nasal capsule (i.e., the cribriform plate); ventral to it is ET II, and an interturbinal (IT) is between them. **D** Here ET II attaches to the roof, and ET III is ventral to it. **E** Most posteriorly, ET III attaches to the roof, and a fourth ethmoturbinal (ET IV) is seen. **F**–**H** In the newborn, the turbinals have started ossification as seen e.g., in the LP of ET I (**G**). Abbreviations: E, eye; LAP, processus anterior of lamina anterior of ET I; LTP, lamina transversalis posterior; PN, paries nasi; SN, septum nasi. Scale bars: 0.5 mm (A–E, shown in A only); 0.5 mm (F, H); 0.1 mm (G).

increases its complexity by a large lamella which attaches dorsally to its stem. It can be regarded as an epiturbinal (Fig. S2C). The most outstanding observation in this specimen is the asymmetry in the posterior part of the olfactory recess, namely a varying number and morphology of its most posterior ETs. The right nasal fossa houses a fourth ET that impedes the caudal expansion of ET III. In the left nasal fossa, the absence of ET IV enables ET III to expand far into the recess (Fig. S2D–F).

In medial 3D view, the overall shape of the turbinal skeleton of the juvenile is similar to the adult (CMZ 930402); including the absence of the anterior process of the LP of ET I which is continuous anteriorly with the LA of ET I (Fig. 3). However, the turbinal shapes differ in coronal view. All turbinals (both laminae of ET I, ET II, ET III, the IT between ET I and ET II, FT 1 to 3) form well-developed single scrolls in the adult. ET I caudally forms a "dorsal" and a "ventral lamina". This separation is not homologous to the LA and LP of ET I, but rather each of them bifurcates dorsally and ventrally independently. Each "dorsal lamina" is continuous within the olfactory recess, and each "ventral lamina" is continuous within the nasopharyngeal duct. ET III expands caudally. ET IV is absent in the adult specimen.

Otolemur ssp.

In a late fetal *O. crassicaudatus* (DLC 2810), three partially or completely cartilaginous ETs have developed (Fig. S3A–E). ET I has extensive ossification of the LA and LP in process (Fig. S3B). The leading edge of the LA of ET I is cone-shaped, with a posteriorly oriented opening. Most caudal structures, including two additional ETs, remain cartilaginous. The FT has commenced ossification anteriorly (Fig. S3A), but remains cartilaginous posteriorly. The LS and PU, and the cribriform plate are undergoing ossification.

In a neonatal specimen (DLC 2824), ossification of all turbinals is nearly or entirely complete (Fig. S3F–I). The anterior process of the LA of ET I is entirely ossified, whereas more caudally the fusion to the cribriform

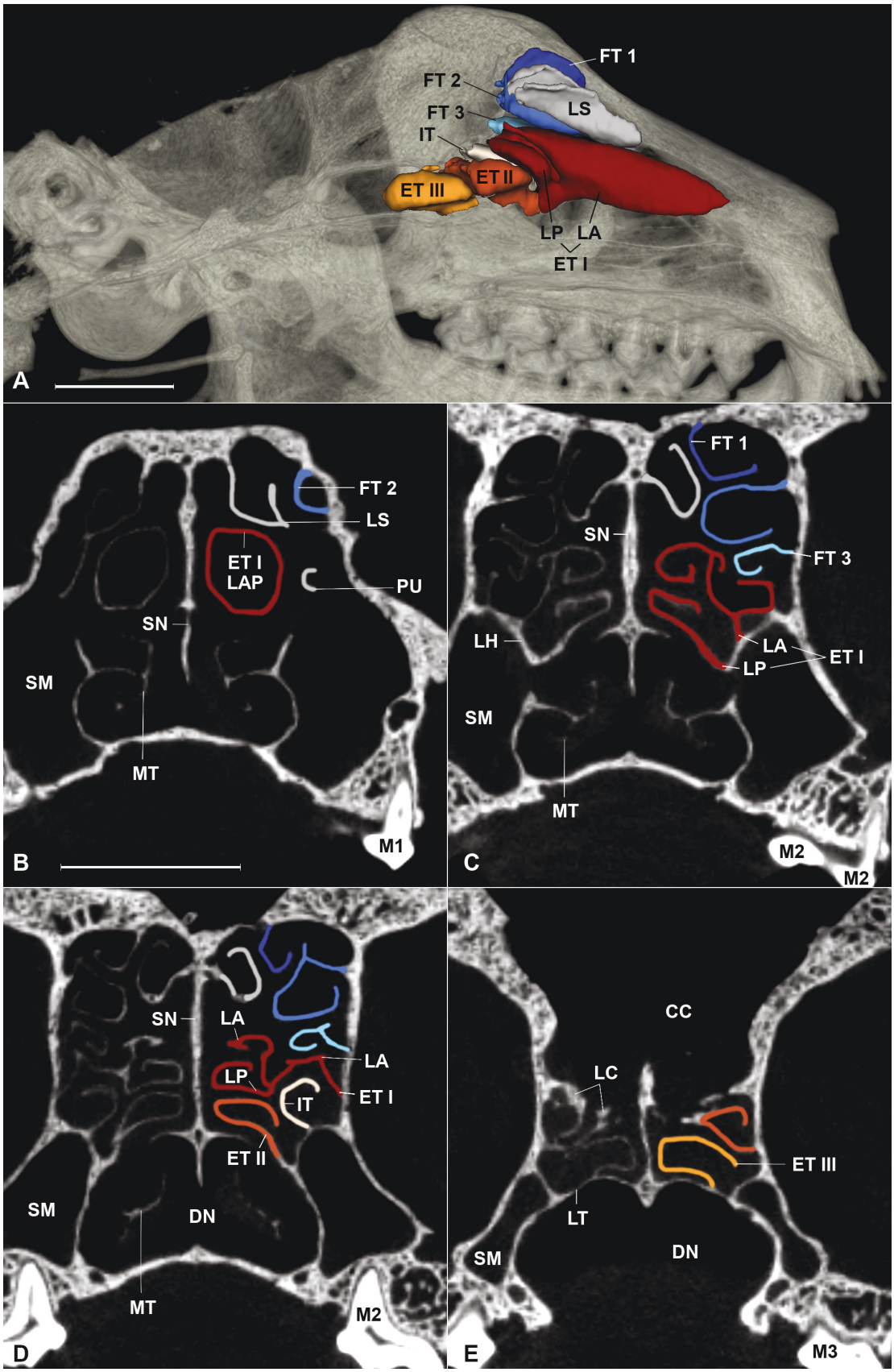

Figure 3. µCT scan of the turbinal skeleton in an adult *Lemur catta* (CMZ 930402). **A** Virtual 3D reconstruction showing the turbinals in medial view in situ within the transparent left nasal fossa. Among primates, *L. catta* retained several patterns of the placental template: ethmoturbinal (ET) I forms an anterior (LA) and a posterior lamina (LP), ET III expands far caudally into the ethmoidal recess, and the pars lateralis houses three frontoturbinals (FTs). **B**–**E** µCT cross sections of the ethmoidal region (rostral to caudal) in rostral view. The turbinals and the semicircular crest (LS) are highlighted. They are well-developed, though their shape remains single scrolled in cross-section. Abbreviations: CC, cavum cranii; LC, lamina cribrosa; LH, lamina horizontalis; LT, lamina terminalis; M1–3, upper 1st to 3rd molar; MT, maxilloturbinal; SM, sinus maxillaris; SN, septum nasi. Scale bars: 5 mm.

plate exhibits some cartilaginous remnants (Fig. S3F, H). Conversely, the anterior process of the LP of ET I retains some "mature" cartilage and has completely ossified caudally. Small parts of the more caudal ethmoturbinals (ET II and III), including parts of the connection to the cribriform plate, remain cartilage. The IT between ET I and II consists of bony tissue only. Similar to the caudal portions of the LA of ET I, hypertrophic chondrocytes and other indications of impending endochondral ossification are identified in the FT (Fig. S3H, I). The LS consists of bone caudally and continues ossification at its rostral end (Fig. S3F, G). The PU has ossification completed.

The ethmoidal region of the infant *O. crassicaudatus* (DLC 2728) houses one FT, three ETs, and one IT between ET I and II (Fig. S4). All turbinals, the LS, and the PU have ossified. The FT, ET III and the lamella attached dorsally to ET II (regarded as an epiturbinal, Fig. S4D–F) form double scrolls in cross-sectional view. The LA and LP of ET I, ET II, and the IT remain simpler single scrolls. The anterior process of the LA of ET I does not only point far rostrally, but stretches ventrally with a mostly simple shape in cross-sectional view. It nearly touches the palate medial to the maxilloturbinal (Fig. S4A–D). The LP of ET I forms an anterior process as well. Caudally, the LA and the LP of ET I as well as ET II each form a "dorsal lamina" and a "ventral lamina" (Fig. S4D, F). The "ventral lamina" of the LP of ET I fuses to the "ventral lamina" of the LA of ET I, and both continue into the nasopharyngeal duct (Fig. S4D). The two individual "dorsal laminae" of the LA and the LP of ET I merge over a short distance and fuse to the cribriform plate separately (Fig. S4D–F). The "dorsal lamina" of ET II connects to the cribriform plate, too. The "ventral lamina" of ET II forms a narrow crest on the transition between the olfactory recess and the nasopharyngeal duct, and ends rostral to the lamina terminalis (see Fig. S4F). ET III expands into the olfactory recess (Fig. S4G). ET II, the epiturbinal attached to it, and ET III form rostral processes similar to ET I (LA and LP). They are cone-like and nested into each other (Fig. S4C, E).

In the adult *O. garnettii* (CMNH-B0748), both laminae of ET I, ET II, ET III, and the IT between ET I and II form well-developed single scrolls in cross-sectional view. The LA and the LP of ET I each forms an anterior process. ET I and II caudally form a "dorsal" and a "ventral lamina", whose topologies are similar to the adult *L. catta* (see above; Fig. S5C, D). The single FT within the pars lateralis is double scrolled (Fig. S5C).

Haplorhini

Platyrrhini

Saguinus spp.

A mid-fetal *S. geoffroyi* (SG10) has a fully chondrified nasal capsule showing no signs of incipient ossification (Figs 4A, 5A–C). There are three ETs (Fig. 4A) which descend as hanging folds. ET I and II cover meatuses, whereas ET III encloses a small recess (Fig. 4A). In the newborn *S. geoffroyi* (SG3) ET I and II are well ossified (Fig. 4B). Ossification is complete in ET II, whereas the dorsal root of ET I remains cartilaginous. There is no trace of ET III visible in the newborn. In the infant (MM105), the ETs appear dorsoventrally more elongated compared to the newborn (Fig. 4C). At all age stages, ET I forms the LA only; the LP is always absent.

In the mid-fetal *S. geoffroyi*, the cupular recess is bordered laterally by the orbitonasal lamina, and ventrally by the lamina transversalis posterior (Fig. 4D). The latter may not ossify or may be the last part of the nasal capsule to ossify, since it is present in a juvenile *S. midas*, and is still typical hyaline cartilage (Fig. 4E, F). In the mid-fetal *S. geoffroyi*, the LS is a small inwardly and downwardly projecting process from the inner side of the nasal side wall (Fig. 5A). The PU descends posteroinferiorly from the LS, with which it is continuous (Fig. 5B), and extends toward the maxilloturbinal; it does not directly contact the maxilloturbinal, but is partially within the same mucosa (Fig. 5C). Both structures are ossified in the newborn and the infant. In the adult *S. oedipus* (So2), the LS is an inwardly and downwardly projecting bony spur (Fig. 5D) and the PU makes the identical downward passage to the maxilloturbinal as seen in the fetus (Fig. 5E, F). In the adult *S. imperator* (M60903; Fig. S6), the LA of ET I forms a "dorsal" and a "ventral lamina" which both fuse to the lateral wall—the "dorsal lamina" rostral to the opening of the olfactory recess, the "ventral lamina" within the nasopharyngeal duct. ET II remains as a solid stretched lamina which does not expand into the lumen with a free margin but instead is attached to the lateral wall in cross-sectional view (Fig. S6C).

Aotus nancymaae

Smith et al. (2023) reported the presence of two ETs in newborn *A. nancymaae* (Aotus108 and Aotus101), and three ETs in an adult (Aotus1). Here, we present additional details. Similar to *Saguinus*, there is no trace of the LP of ET I in any of the investigated specimens. In the newborn Aotus108, both ETs are confirmed to be products of endochondral ossification because they remain partly cartilaginous (Fig. 6A–D). The LA of ET I and ET II each form an anterior process, which caudally continues into a straight lamina in coronal view. Caudally, both ETs divide into a "dorsal lamina" continuing into the olfactory recess dorsal to the transverse lamina, and a "ventral lamina," which runs ventral to the transverse lamina into the nasopharyngeal duct, though the "ventral lamina" of ET II is a narrow crest (Fig. 6C). The topology of ET I and II does not change in the older stages. The LS in newborn Aotus101 has a small amount of cartilage remaining on its very anterior end, the remainder of the LS and the entire PU is ossified in this specimen. In the Aotus108, the entire LS and PU is ossified.

Ossification of the entire turbinal skeleton including the LS and the PU is completed in the 14-day-old Ao-

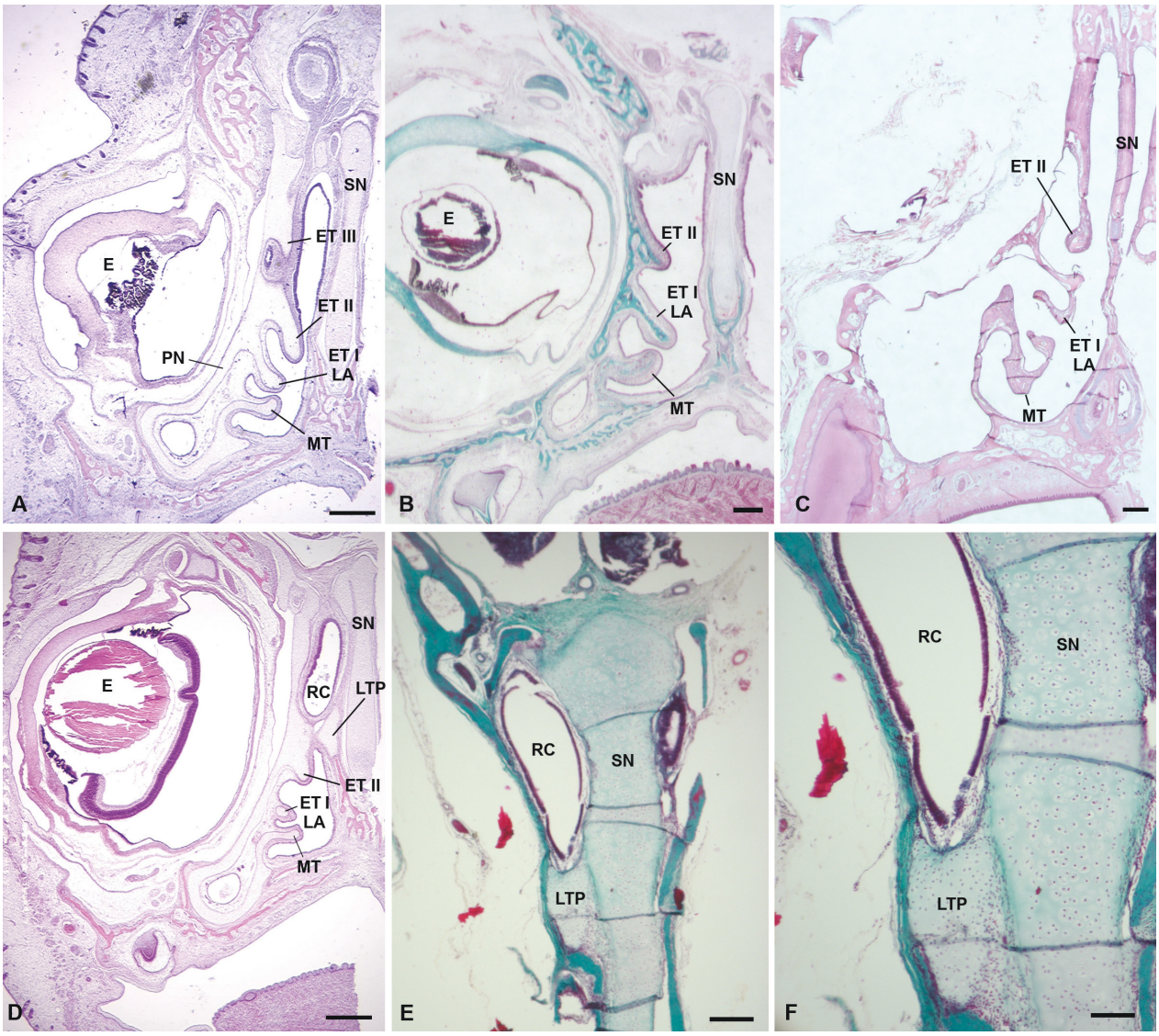

Figure 4. Histological serial sections of the nasal capsule in tamarins (*Saguinus* spp.) in coronal view (rostral to caudal). **A** Mid-fetal *S. geoffroyi* (SG10) showing an entirely cartilaginous nasal capsule, in which three ethmoturbinals (ET I, II, and III) are visible. **B** In a newborn *S. geoffroyi* (SG3), only two ETs are seen, and both are at least partly ossified. **C** In an older infant *S. geoffroyi* (MM105), two ETs are present and are projected to a greater degree (**C**). Figs D through F are sectioned through the cupular recess (RC), which is supported ventrally by the posterior transverse lamina (LTP). In the fetus (**D**) the LTP ends posteriorly as an isolated cartilaginous process. **E**, **F** In a juvenile *S. midas* (Smidas), the LTP remains partially cartilaginous. Abbreviations: E, eye; LA, lamina anterior of ET I; MT, maxilloturbinal; PN, paries nasi; SN, septum nasi. Scale bars: 0.4 mm (A, D); 0.5 mm (B, C); 0.2 mm (E); 0.1 mm (F).

tus104. In the two older infants (Aotus107 and Aotus102, Fig. 6F), an increase of surface area occurs; most certainly based on appositional bone growth. But the turbinal morphology does not become markedly more complex. Aotus104, Aotus102, and the adult (see above) possess an additional third ET, which is positioned dorsal to the transverse lamina within the olfactory recess. It develops as a small osseous bulge in Aotus104 (Fig. 6E) and stretches to a dorsally pointing lamina in the adult (Fig. 6G). Histology of Aotus104 indicates that the bulge constituting ET III is only supported by bone. Much of the nasal side wall is already resorbed or ossified at this age; in the vicinity of ET I, only an island-remnant of the nasal side wall remains (Fig. S7).

Though Aotus107 and Aotus102 are at a similar stage of dental development (all deciduous teeth in occlusion, M1 starting to erupt), an osseous ET III was not confirmed in the µCT scan of Aotus107. Histological data are not yet available to reveal whether ET III is completely absent or might be present as a small epithelial bulge.

The three ETs form simple single scrolls in the adult Aotus1, though the "ventral lamina" of the LA of ET I complicates to a dendritic-like shape (Fig. S8B, C). The narrowed space of the nasal cavity caused by the enlarged orbits forces ET I and II to caudally form a "dorsal lamina" and a "ventral lamina" (Fig. S8D, E). The former continues into the olfactory recess, whereas the latter expands ventral to the lamina terminalis into the pars anterior and the nasopharyngeal duct (Fig. S8E). Because the rostral end of ET III does not reach notably rostral to the lamina terminalis, ET III is entirely positioned dorsal to it (Fig. S8E).

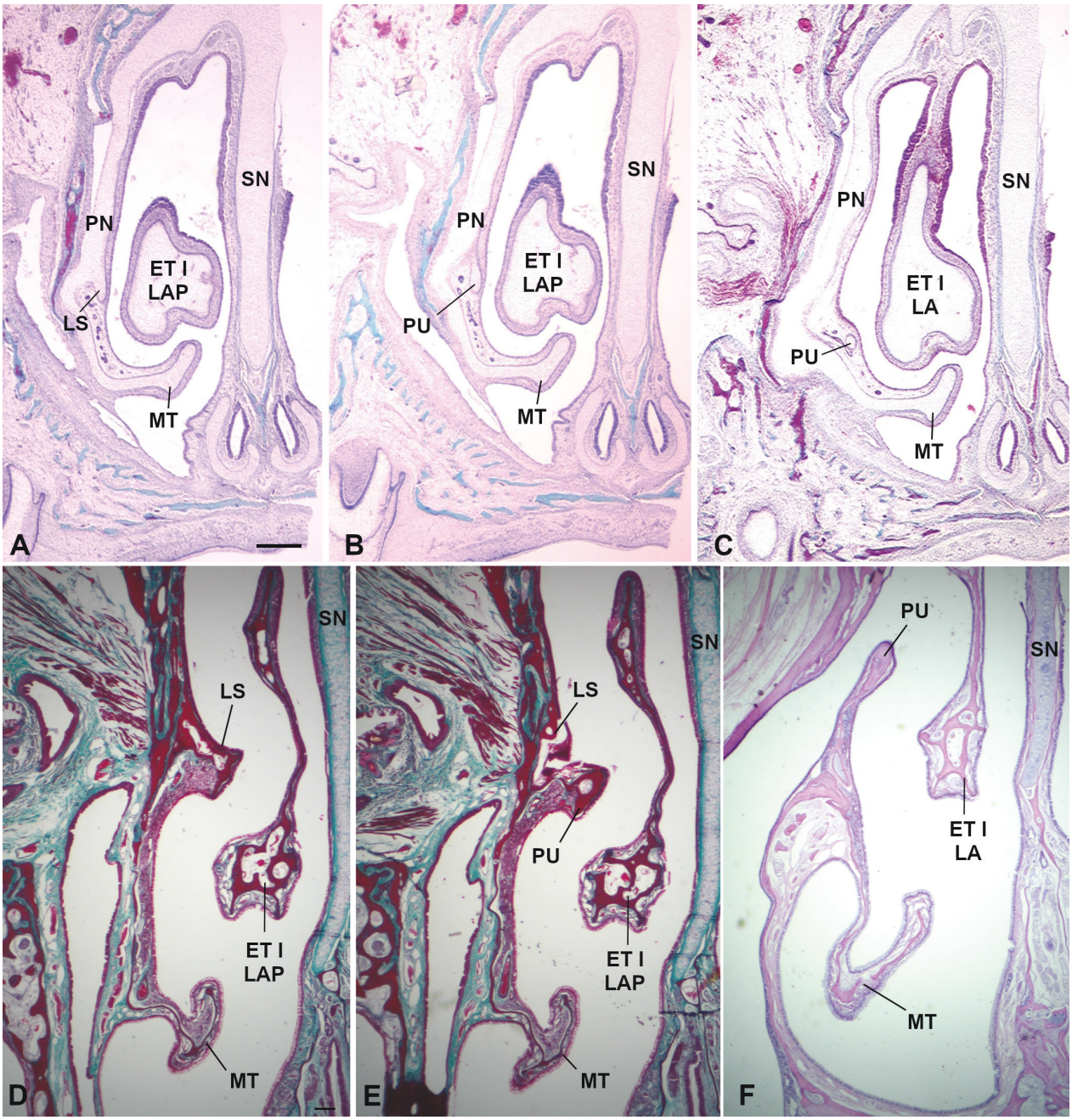

Figure 5. Histological serial sections (rostral to caudal) of the semicircular crest (LS) and uncinate process (PU) in tamarins (*Saguinus* spp.) across age. **A**–**C** Mid fetal *S. geoffroyi* (SG10) showing the LS as a ridge projecting inward from the nasal side wall (PN). The PU projects posteroventrally toward the maxilloturbinal (MT) from the LS (**B**, **C**). **D**–**F** The same spatial relationship is seen in an adult *S. oedipus* (So2). Note that the PU does not articulate directly with the MT (**F**). Abbreviations: ET I, ethmoturbinal I; LA, lamina anterior of ET I; LAP, processus anterior of the LA of ET I; SN, septum nasi. Scale bars: 0.2 mm (scale bar in A and D apply to the entire row).

Pithecia pithecia

In the histologically sectioned newborn *P. pithecia* (Saki2), the LS is a downwardly projecting spur (Fig. S9A). It is cartilaginous anteriorly, and ossified for most of its middle region. The PU descends from it and is sickle shaped and partially cartilaginous (Fig. S9B). Near the maxilloturbinal it becomes completely cartilaginous (Fig. S9C). The ET I (LA, the LP is absent) is cartilaginous near its connection to the lateral wall, but is otherwise well ossified throughout its length. No ET II is apparent. Since only every tenth section was stained, it is possible the turbinal is present but small enough to exist between stained sections. A second *P. pithecia* newborn (Saki3) reveals a similar ET I and ET II as a small epithelial bulge (Fig. S9D–F), though the composition of ET II as bone, cartilage, or only loose connective tissue is unclear based on the diceCT data.

The adult *P. pithecia* (CMNH-11-F3) exhibits a pattern in the three ETs similar to the adult *A. nancymaae* (see above), though the ETs are markedly reduced in size (Fig. S10). In particular, ET II and III appear as narrow

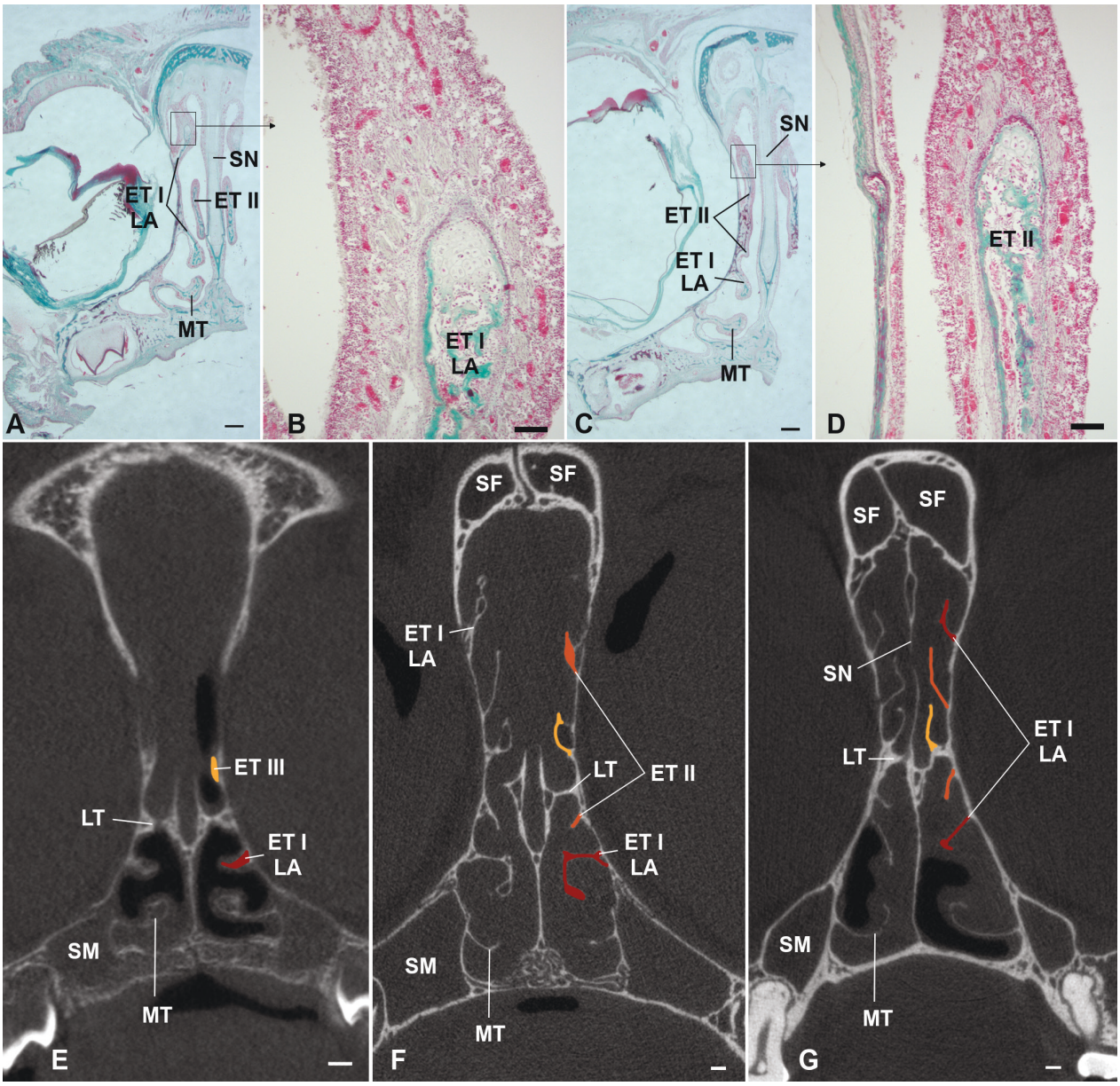

Figure 6. Ethmoidal region of cross-age series of the night monkey (*Aotus nancymaae*) in coronal view. **A**–**D** Histological serial sections of a newborn (Aotus108). Shown are the first and second ethmoturbinal (ET I, II) (**A**, **C**), and enlarged views of each (**B**, **D**); note some cartilage remains (*) in both turbinals. No ET III is visible in any newborn in our sample. **E**–**G** Coronal µCT slices in rostral view in that the ETs are highlighted on the left side of the nasal fossa. ET III is visible as a bony ridge in a 14-days-old *A. nancymaae* (Aotus104) (**E**), and is more elongated in an older infant (Aotus102; with full deciduous eruption) (**F**), and in an adult (Aotus1) (**G**). Abbreviations: LA, lamina anterior of ET I; LT, lamina terminalis; MT, maxilloturbinal; SF, sinus frontalis; SM, sinus maxillaris. Scale bars: 1 mm (**A**, **C**); 0.1 mm (**B**, **D**); 0.5 mm (**E**–**G**).

ridges along the lateral wall and do not expand as far caudally as ET I, which continues as far into the nasopharyngeal duct as the maxilloturbinal (Fig. S10D, E).

Catarrhini

Macaca spp.

Previously, Maier (2000) described a fetal *M. fascicularis* (CRL 55 mm) with a fully chondrified nasal capsule showing no signs of incipient ossification (Fig. S11). This specimen possesses two ETs—ET I forms only the LA but no LP—and a LS. However, no PU was described by Maier (2000).

A newborn *M. mulatta* (YN09-175) in our sample possesses two fully ossified ETs; the LS and the PU are fully ossified as well. A subadult *M. nemestrina* (516-A6; no recorded age; incomplete deciduous eruption) possesses two ETs and the LS, which forms the PU (Fig. S12). All named structures are fully ossified. The LA of ET I is straight in cross-sectional view and points ventrally. It forms an anterior process. The LP of ET I is absent. ET II is reduced to a short and narrow crest (Fig. S12C).

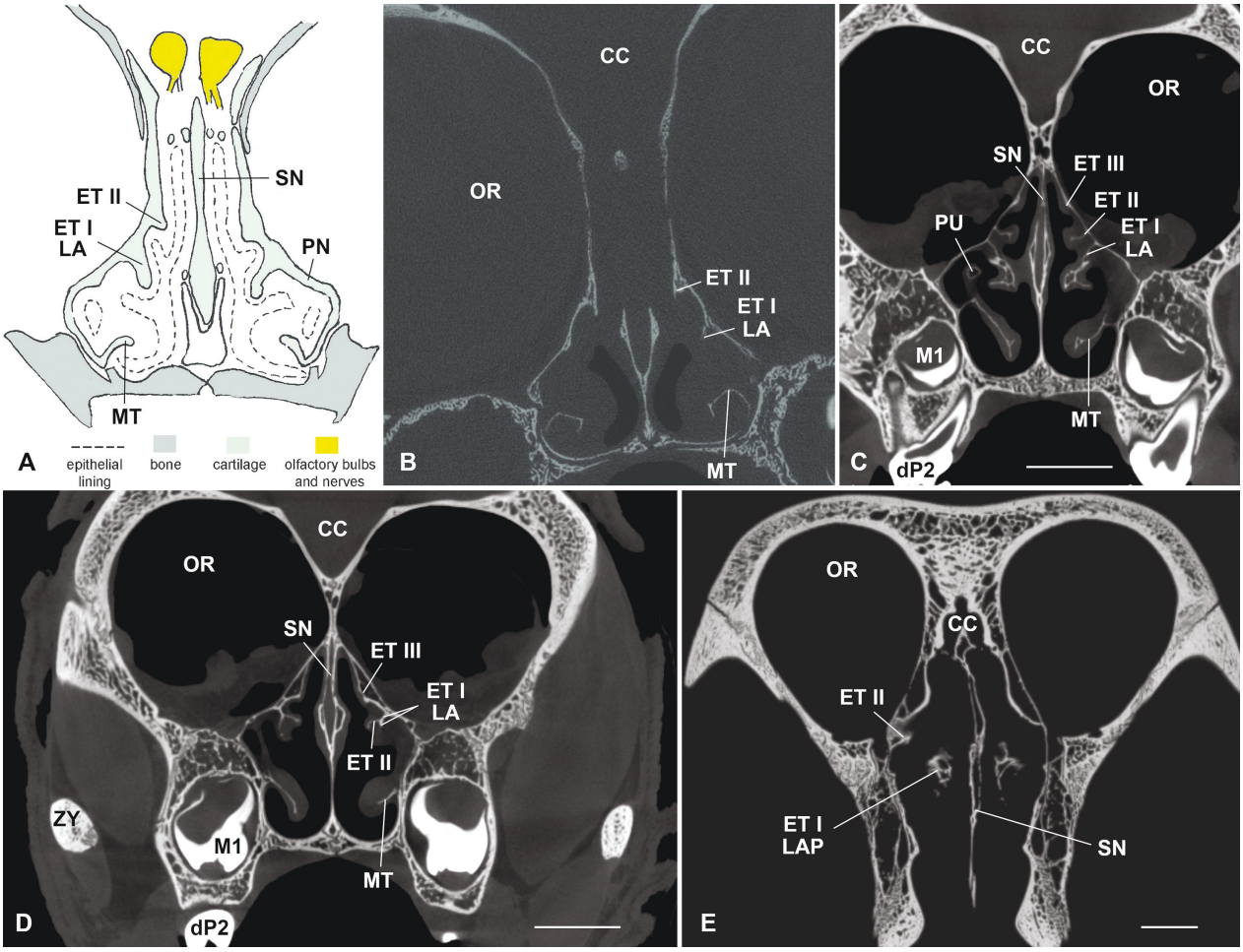

Figure 7. Ethmoturbinal region in baboons (*Papio anubis*) across age, viewed in a coronal plane. **A** Schematic illustration of a mid-fetal specimen (CRL 115 mm), redrawn after Maier (2000, fig. 5.4, serial section # 165). Two ethmoturbinals (ET I, II) are indicated in this section. **B** Late fetal specimen (Papio107, 150 days gestation), showing an ossified ET I and II in a similar position to the earlier stage fetus. **C**, **D** One year, 32 days old specimen (Papio108), showing more fully grown ET I and II (**C**). More posteriorly, a third ethmoturbinal (ET III) is visible as a small mucosal bulge only, with a small spur within it (**D**). **E** Adult individual (amnh:mammals:m-51380) showing the rostrally elongated ET I, and ET II. Abbreviations: CC, cavum cranii; dP2, deciduous upper 2nd premolar; LA, lamina anterior of ET I; LAP, processus anterior of the LA of ET I; M1, upper 1st molar; MT, maxilloturbinal; OR, orbita; PN, paries nasi; PU, processus uncinatus; SN, septum nasi; ZY, zygomatic. Scale bars: 10 mm.

The LA of ET I expands far rostrally in the two adults *M. fascicularis* (mcz:mamm:23812) and *M. mulatta* (MCZ:Mamm:26475), and in the adolescent *M. nemestrina* (A3) due to their prognathic face (Smith et al. 2014b; Fig. S13). In cross-sectional view, the LA of ET I forms a bulbous anterior process and continues posteriorly as a simple, non-diversified, and ventrally pointing lamina (see e.g., Fig. S13J–L). ET II is hard to identify in all three specimens because it is reduced to a narrow ridge (Fig. S13D, K).

Papio anubis

A fetal *P. anubis* previously described by Maier (2000) has a fully chondrified nasal capsule (Fig. 7A). This specimen possesses two ETs, the LP of ET I is absent throughout the *Papio* sample. The PU has started to ossify distally, but the two ETs remain cartilaginous. In our sample, ossification of ET I and II appears complete even in the late fetus (Papio107), and they retain the simple morphology of a hanging fold through future development (Fig. 7B). In the older infant Papio108, ET I forms a small lamella extending ventrolaterally from the basal lamina (Fig. 7C). ET I and II merge posteriorly, whereas a third ET is seen in the form of a small ridge (Fig. 7D). A major distinction from the older infant is the marked rostral outgrowth of ET I in the adult *P. anubis* (amnh:mammals:m-51380; Fig. 7E). The shape and topology of ET I is similar to the three *Macaca* species (see above, Fig. S14). ET II forms a short ridge (Fig. S14D).

In the fetal *P. anubis*, the LS projects inward and downward from the nasal side wall. A PU was observed by Maier (2000); similar to the mid-fetal *S. geoffroyi*, the PU continues posteroventrally into the same mucosa as the maxilloturbinal (Fig. 8A). The LS and the PU are ossified in the late fetus (Fig. 8B), and occupy a similar position across the age (Fig. 7B–D).

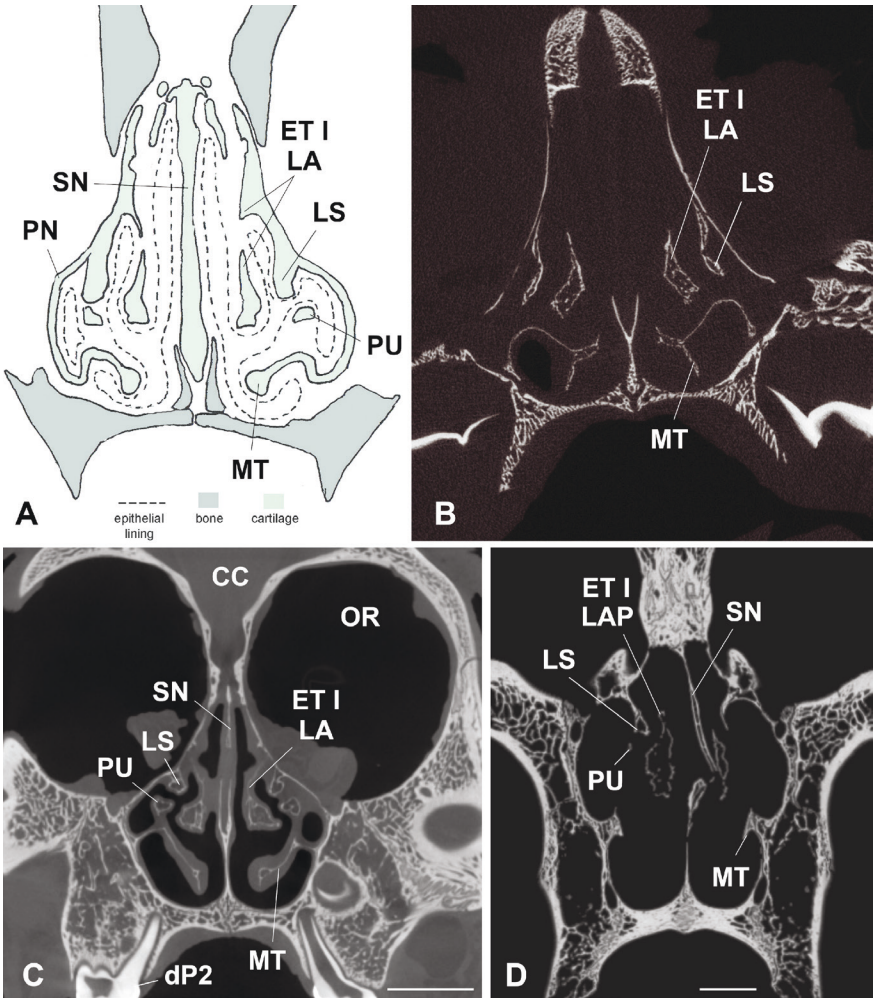

Figure 8. The semicircular crest (LS) and uncinate process (PU) in baboons (*Papio anubis*) across age, viewed in a coronal plane. **A** Schematic illustration of a mid-fetal specimen (CRL 115 mm), redrawn after Maier (2000, fig. 5.4, serial section # 124-2). The cartilaginous LS and PU are visible. **B**–**E** µCT cross sections of the ethmoidal region. **B** Late fetal specimen (Papio107, 150 days gestation), showing an osseous LS. **C** One year, 32 days old specimen (Papio108), showing an ossified LS and PU. **D** Adult individual (amnh:mammals:m-51380) showing both structures. Abbreviations: CC, cavum cranii; dP2, deciduous upper 2nd premolar; ET I, ethmoturbinal I; LA, lamina anterior of ET I; LAP, processus anterior of the LA of ET I; MT, maxilloturbinal; PN, paries nasi; SN, septum nasi. Scale bars: 10 mm.

Ontogenetic states

In Strepsirrhines, the first structures of the turbinal skeleton, which start to ossify are the two laminae of ET I (LA and LP), and the LS with its associated PU (Fig. S15). The rostrally positioned PU is the first structure to complete ossification in both *L. catta* and *O. crassicaudatus*, whereas in the LS, ET I, and all more posterior turbinals endochondral ossification is still proceeding. All turbinals which are present in the ossified ethmoid emerge from the paries nasi within the cartilaginous nasal capsule (Fig. 9), and have completely replaced the cartilaginous precursors before adulthood (Fig. S15).

Among platyrrhines (Fig. S16), endochondral ossification is nearly complete in the neonate *S. geoffroyi*, whereas in the similar-aged *A. nancymaae* and *P. pithecia* all turbinals, the LS, and the PU are still partly cartilaginous. Most conspicuously, in one neonate *P. pithecia* (Saki3), ET II is even at the earliest state of an epithelial bulge. Nevertheless, ossification proceeds comparatively fast at least in *A. nancymaae*, because ET I to III, the LS, and the PU are completely osseous in the 14-days-old Aotus104. The most striking variation is the heterogeneous turbinal pattern between the cartilaginous template and the ossified ethmoid, namely the presence of a cartilaginous ET III in the mid-fetal *S. geoffroyi*, whereas this turbinal is entirely absent in all postnatal stages after ossification has begun (Fig. 9). In *A. nancymaae* and *P. pithecia*, the opposite is observed, namely the absence of ET III in the neonates, whereas it is present as bone in older stages.

In the two investigated catarrhine species ossification is complete at birth (*M. mulatta* YN09-175) or already before birth (*P. anubis* Papio107) (Fig. S16). Whereas the PU was not observed at the youngest *Macaca* stage by Maier (2000), the PU is the first structure undergoing endochondral ossification in the fetal *P. anubis* (Maier 2000). In all other *Macaca* age stages in this study, a bony PU is present. In contrast to platyrrhines, the number of turbinals remains constant throughout development (two ETs in *Macaca* spp. and *P. anubis*) (Fig. 9); except the presence of a bony ET III in the older infant Papio108.

Discussion

The therian—and derived primate—grundplan

The tripartite nasal capsule of the therian grundplan consists of the pars anterior (maxilloturbinal, nasoturbinal), the pars posterior (ETs, ITs), and the pars lateralis (FTs,

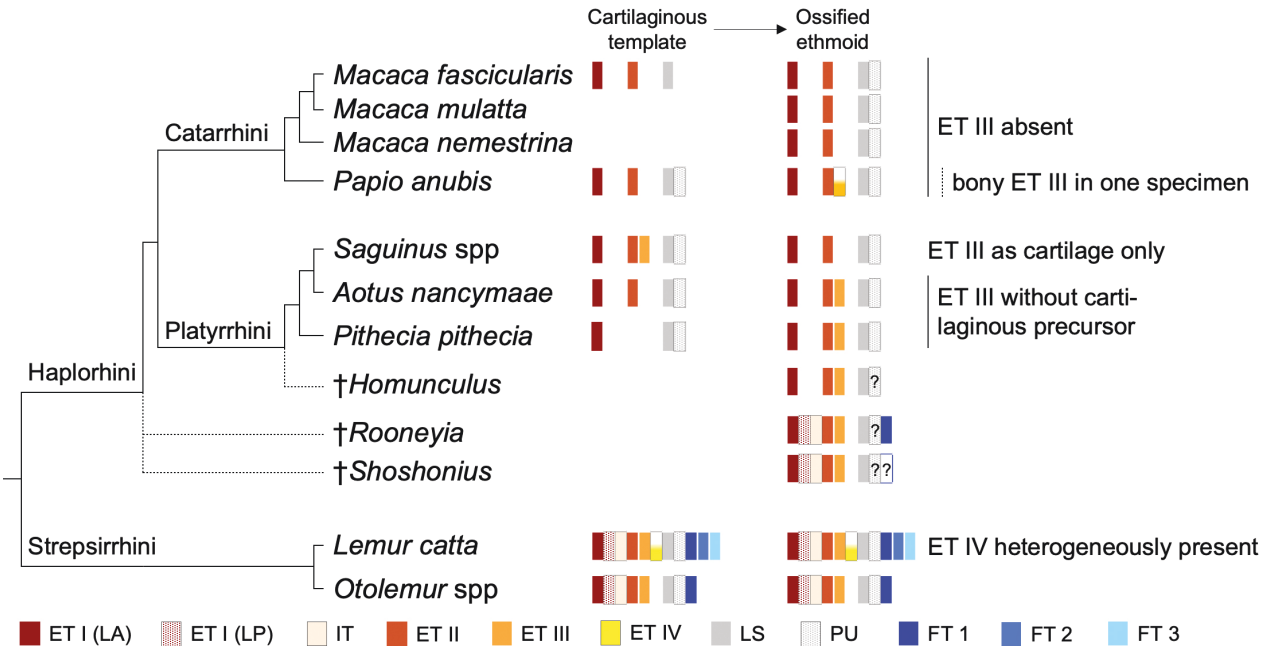

Figure 9. Phylogenetic tree (see Fig. 1 for reference) of the examined primates, that is expanded by three fossil species (dashed lines, topology according to Lundeen and Kirk 2019 for *Rooneyia*, Kirk and Lundeen 2020 for *Shoshonius*, and Lundeen and Kay 2022 for *Homunculus*). The presence of the turbinals within the cartilaginous nasal capsule during early development and within the ossified nasal cavity at late development are shown (for details on the individual age stages see Figs S15, S16). Strepsirrhines exhibit the plesiomorphic pattern of three ethmoturbinals (ET I to III; up to ET IV in some *L. catta* specimens) and one interturbinal (IT) between ET I and II. The plesiomorphic number of frontoturbinals (FT 1 to FT 3) remains yet unknown. In contrast, all haplorhines are recognized by the absence of all FTs, the IT, and the posterior lamina (LP) of ET I, which all have been present in stem haplorhines represented by *Rooneyia* (Lundeen and Kirk 2019) and *Shoshonius* (Kirk and Lundeen 2020). Whether the damaged pars lateralis of the examined *Shoshonius* specimen housed FTs cannot be assessed (Kirk and Lundeen 2020). The stem platyrrhine *Homunculus* housed three ETs in its nasal cavity (Lundeen and Kay 2022), whereas among extant platyrrhines ET III exhibits a markedly heterochronic pattern. The most distinctive observation is the presence of a third ET in the cartilaginous template of *Saguinus*, which is absent in the ossified ethmoid, and on the other hand the absence of ET III in the nasal capsule of *Aotus* and *Pithecia*, whereas a bony ET III-like lamina was identified after ossification of the nasal region has completed. The presence of an uncinate process (PU) in the fossils is not evident from the literature. Abbreviation: ET I (LA), lamina anterior of ET I.

ITs); the latter is rostrally separated by the LS, a posterior projection of the lateral wall of the pars anterior (Voit 1909; Reinbach 1952a; Smith and Rossie 2008; Martinez et al. 2024b). Primates are visual specialists, and the stereoscopic orbits which enable a depth perception are closely linked to the shape of the nasal capsule which in turn functions as a temporary template ("Stemmkörper") for the enclosing dermal bones (Maier 1993b, 2000; Smith et al. 2014b). If we assume that the basal placentals' pars posterior housed three ETs and an IT between ET I and II (Schrenk 1989; Ruf 2014), strepsirrhines conserved the plesiomorphic number (Fig. 9). It is also possible that the placental grundplan exhibited four ETs, in which case ET IV became lost in crown primates. Our assumed number of three to four ETs and an IT between ET I and II for the earliest primates agrees with Lundeen and Kirk (2019). However, the plesiomorphic number of FTs remains so far unresolved, but for basal Euarchontoglires (Fig. 1) two FTs are supposed to have been present in the pars lateralis (Maier and Ruf 2014). Lundeen and Kirk (2019) also assert that two FTs might be the primitive condition for Euarchonta, but they point to a possible homoplastic pattern with regard to the variable FT number within strepsirrhines. Their assertion is confirmed by our data and other studies, reporting a range from one (e.g., *O. garnettii*, present study) to three FTs (*L. catta*, present study; *Daubentonia*, Maier and Ruf 2014).

Strepsirrhines (*Otolemur* and *Lemur*, present study; *Daubentonia*, Maier and Ruf 2014) exhibit a distinctively higher number and complexity of turbinals compared to haplorhines, though the current descriptive data need to be confirmed by morphometric analyses. On the contrary, the great degree of orbital convergence in platyrrhines and catarrhines (Ross 1995) compresses the olfactory recess and the ETs. Further, a rostro-caudal compression is associated with the reduced midfacial length (Smith et al. 2014b). In both haplorhine groups, the constrained space coincides with (1) the reduction of the pars lateralis with an associated loss of all FTs; (2) the narrowing of the ethmoturbinal recess which forms the caudal end of the nasal cavity dorsal to the transverse lamina; and (3) the simplification and size reduction of ETs to narrow ridges (Maier 1993b; Smith et al. 2014b).

Individual turbinals are still difficult to homologize among placental taxa because a comprehensive developmental pattern across a vast species sample is still lacking

(Maier 1993b; Werneburg et al. 2013). However, ET I is identifiable in all mammals (excepting those that have lost turbinals) by virtue of its relationship with the rest of the nasal capsule. Its LA overlaps the pars intermedia and juts rostrally as the antero-most element of the pars posterior (e.g., Lagomorpha, Ruf 2014; *Canis*, Wagner and Ruf 2019, 2021; Chiroptera, Ito et al. 2021; Eulipotyphla, Ito et al. 2022). The spatial relationship in all therians makes its homology exceedingly likely. Although perhaps less certain, the LP of ET I (ET II, for some authors) likewise has consistent spatial relationships across many mammals suggesting homology. This element shares a basal lamella, at least for part of the nasal cavity, with the LA (e.g., Paulli 1900a, 1900b, 1900c; Maier 1993a; Smith and Rossie 2008; Macrini et al. 2023). Strikingly, no such turbinal bears this relationship to the LA of ET I in any haplorhine studied here. The second lamina within the pars posterior does not fuse to ET I and merges with the cribriform plate as an independent turbinal. This pattern corresponds to the topology observed in ET II in the therian template (Paulli 1900a, 1900b, 1900c). We confirm Maier's (2000) identification of the second lamina within the pars posterior as ET II, though he highlighted that it might possibly be the LP of ET I. This leads us to infer that the LP of ET I is lost in haplorhines, as suggest by others (e.g., Maier and Ruf 2014), and as apparently occurs in parallel in many bats (Ito et al. 2021). We hypothesize that the LP of ET I, being a far smaller element than the LA, is more prone to phylogenetic loss. This will require testing using a broader sample of mammals across developmental age, while taking phylogeny into account (e.g., *Homunculus*, see below). Similarly, the catarrhine template is lacking ET III, though it is present in one *Papio* specimen (see below). Our current study of primates suggests that reduced and simplified structures may also be properly recognized if their ontogeny is thoroughly investigated (turbinals, Maier 1993b; teeth, Hautier et al. 2016), even though the identity of lost elements is not always certain. Indeed, inferences about the loss, gain, or possible fusion vs. duplication of specific turbinals still remain largely unresolved (Smith and Rossie 2008; Van Valkenburgh et al. 2014).

Whereas within the pars posterior ET I, ET II and the IT in-between are quite easily distinguished, the terminology within the pars lateralis remains obscure. The investigated age series in *L. catta* did not provide any differentiation between FTs and ITs. As in the youngest available stage (fetal) all three turbinals exhibit a similar size, single-scrolled shape, and topology, we identified them as three FTs. In the infant however, ossification is most advanced in FT 2 that projects the most rostrally. FT 1 is at the least advanced stage of ossification. Based on the present sample, it is so far impossible to elucidate which FT in *L. catta* might be homologous to the single FT in *O. garnettii*. For instance, the three FTs remain simple single scrolls in the adult *L. catta*, whereas in *O. garnettii* the FT is more complex (double scroll). We adapted the scheme emphasized by, e.g., Smith and Rossie (2008) and simply counted the turbinals from medial (turbinal next to LS labeled as FT 1) to lateral/ventral in *L. catta*. Similarly, *O. garnettii* houses a single FT within its pars lateralis, designated as FT "1" based solely on position and not necessarily homology.

Phylogeny

The pars posterior of the two fossil primates *Shoshonius cooperi* (early Eocene) and *Rooneyia viejaensis* (late middle Eocene) housed three ETs (including the LP of ET I) and an IT between ET I and II (Fig. 9). Whereas *Rooneyia* exhibited one FT, the presence of turbinals within the largely damaged pars lateralis of *Shoshonius* remains yet unknown. Though the number and the complex morphology of all turbinals was more similar to strepsirrhines, both species were regarded as stem haplorhines (Lundeen and Kirk 2019; Kirk and Lundeen 2020). The Miocene *Homunculus patagonicus* represents a stem platyrrhine which conserved three ETs, whereas the LP of ET I, the IT between ET I and II, and the pars lateralis were absent (Lundeen and Kay 2022) (Fig. 9). The turbinal surface area was larger compared to extant platyrrhines (Lundeen and Kay 2022), and the morphology in cross-section most closely resembled that of adult Aotus1 in our sample. Though all adult catarrhines and one platyrrhine (*S. imperator*) are lacking ET III, we observed an osseous ET III in an infant *P. anubis* (Catarrhini) and a cartilaginous ET III in a mid-fetal *S. geoffroyi* (Platyrrhini). On the other hand, in the two platyrrhines in which ET III is present in adults (*P. pithecia*, *A. nancymaae*) the neonate nasal capsule shows no evidence of a cartilaginous or ossifying third ET (Fig. 9). The heterogeneous presence of ET III could result from two different evolutionary scenarios:

(1) Phylogenetic constraints. ET III has become lost convergently in catarrhines and platyrrhines due to its presence in *Homunculus* (Lundeen and Kay 2022) and the young *S. geoffroyi*. In *S. geoffroyi*, the cartilaginous ET III gets resorbed instead of ossifying, which might represent a transitional state of undergoing turbinal loss. On the other hand, in *A. nancymaae* and *P. pithecia* ET III does not emerge from a cartilaginous precursor within the nasal capsule but instead develops through appositional outgrowth after the cartilaginous nasal sidewall has largely been resorbed. This implies a different developmental origin of ET III—and in *P. pithecia* additionally of ET II—and reveals an apomorphic condition compared to turbinals formed from the cartilaginous nasal capsule at an earlier ontogenetic stage. Our observation too might explain the smaller size and varying topology of ET III in *A. nancymaae*, namely its position dorsal to the transverse lamina, which develops at an earlier ontogenetic stage as result of the ossified lamina transversalis posterior (partly connecting with the ossified vomer, Smith et al. 2021b). Similarly, ET II and III are conspicuously smaller compared to the endochondrally ossified ET I (LA) in *P. pithecia*, even though they partly continue into the nasopharyngeal duct ventral to the transverse lamina.

The phenomenon of ET III appearing in some platyrrhines is striking. Since ET III is not present as a cartilaginous structure in newborns of *A. nancymaae*, nor is it an osseous lamella at birth, we infer that it is absent in the cartilaginous template. There are other examples of portions of turbinals forming without cartilaginous precursors. Smith et al. (2016) surmised that tertiary lamellae of maxilloturbinals in some strepsirrhines form as bony outgrowths from nonchondrally ossified turbinals. Whereas the appositional nature of these accessory lamella was an inference based on comparisons of infants to adults (Smith et al. 2016), our *Aotus* sample appears to form the entire ET "III" through progressive stages of development. At birth, no trace of either a cartilaginous or osseous ET "III" is seen. In an early infant stage, ET "III" appears to be only a bony ridge (Fig. 6E). In one of the older infants, ET "III" is a small, upwardly projecting bony spur, appearing to be a smaller precursor to ET "III" of the adult, an upwardly projecting bony fold (Fig. 6F, G). Since such bone forms as appositional outgrowth of existing endochondral bone, Smith et al. (2016) noted a similarity to the occurrence of membranous bone that emanates away from the cartilaginous cranial base during fetal development, called Zuwachsknochen in the German literature (e.g., Maier 1993a). Recently, DeLeon et al. (2022) suggested the term "ectochondral" bone for bones that ossify from endochondral bone before or after it ossifies. It is contextually distinct from intramembranous bone which forms earlier in development, with no precursor. Ectochondral bone, in contrast, is a means of elaboration of osseous structure at fetal or later stages of development. As such, ectochondral bone (a.k.a., Zuwachsknochen) may be an especially important means for generating novel osseous structures, or in this case, "reacquisition" of a third ET.

Unlike the third ET described above for some haplorhines, in strepsirrhines with presumably derived additional turbinals, these structures were intrinsically part of the cartilage template. For example, the suggested apomorphic third FT in *L. catta* emerges from a cartilaginous precursor. This observation may imply either that varying turbinal numbers are based on heterochronic developmental timing (early as cartilage, or late as bone) or that stem primates (or earlier lineages up to therians) housed three FTs in their pars lateralis.

(2) Intraspecific variation. Previous studies asserted that there is a species-specific number of ETs and FTs (e.g., Ruf 2014; Wagner and Ruf 2021). However, the use of different terminologies impedes a generalization of this observation. For instance, Smith et al. (2016) observed a variation of turbinal number within the pars lateralis in three *L. catta* specimens (three vs. four); they were identified as FT1 to FT3 and FT4, respectively. The authors emphasized that two turbinals were conspicuously larger (apparently called FT1 and FT2), indicating that the smaller turbinals were more likely ITs whose number varies between one and two. Similarly, Macrini (2012) observed two and three ectoturbinals within one *Notoryctes* skull; suggesting that, beside two FTs, the third ectoturbinal may be an IT that is missing on one side of the nasal fossa. Our own observation of a variable ET number within the nasal cavity of a juvenile *L. catta* (four in the right and three in the left nasal fossa) further refutes the theory of uniform ET – and similarly FT – numbers among placental species; indicating that ETs, at least, might be subject to intraspecific variation.

Despite the still ongoing debate about a vision-olfaction tradeoff, morphological reduction may characterize all haplorhines and even most strepsirrhines (though to a lesser degree in the latter group) (Smith and Bhatnagar 2004; Smith et al. 2004, 2014a, 2019; Melin et al. 2009; Lundeen and Kirk 2019). A relaxed or neutral selective pressure promotes variation (polymorphism) of a structure (Darwin 1859), in the present example the turbinal skeleton. Evidence for this assertion is provided by the CT scans of adult *P. pithecia*, in which one specimen exhibited one ET, the second two ETs, and the third two ETs on one side of the nasal fossa and three on the other side (unpublished data). A field study confirmed that *P. pithecia* prefers unripe fruits, which emit low levels of aldehydes and are hence primarily selected based on visual stimuli (Urbani 2002). In this context, it may be critical to realize that anthropoids (at least platyrrhines) distribute much olfactory epithelium on non-turbinal surfaces, such as the septum and "roof" of the nasal cavity (Smith et al. 2004). Some authors suggest numbers of turbinals are unreliable proxies for olfactory capabilities, at least in some mammals (e.g., Wagner and Ruf 2019, 2021; Martinez et al. 2023, 2024a, 2024b). This may be the case for anthropoid primates as well.

Beside the turbinal number, the reduced nasal cavity in haplorhines affected the morphology of the ETs, which either simplify or remain less complex single scrolls, up to double scrolls at most, in cross-sectional view. Since the turbinals in tree shrews (Scandentia) have a larger surface area compared to primates and colugos (Dermoptera), a simplification linked with a decreased surface area of the turbinal skeleton in Primatomorpha seems evident (Lundeen and Kirk 2019) (Fig. 1). However, to our best knowledge, hypotheses about the plesiomorphic turbinal shape in placentals are scarce, although Lundeen and Kirk (2019) inferred that the ancestral morphology of ethmoturbinals in primates is bullar.

Due to lack of certainty about homology, ETs and FTs are still simply counted according to their growth series from rostral (ET I and FT 1) to caudal throughout the species. A particularly challenging terminology refers to structures in the pars lateralis, because FTs and ITs are difficult to distinguish, especially when pre-adult stages are lacking.

The current sample neither confirms nor refutes the assumed number of two FTs in basal Euarchontoglires (Maier and Ruf 2014). Assuming that number is correct, in *L. catta* a third FT emerged, *O. garnettii* lost one FT. We need to enlarge the sample of strepsirrhine species and to include more ontogenetic series to receive reliable evidence of evolutionary changes within this lineage's pars lateralis (e.g., which FT is lost or gained).

Challenges for phenotypic analyses and trait recording

The use of morphological traits of the nasal cavity in phenotypic studies (e.g., associations with OR genes, Christmas et al. 2023) requires their homology across the species. As early developmental stages closely resemble the placental template, they enable the reliable identification of individual structures of the intranasal skeleton (Reinbach 1952a, 1952b). Provided that comprehensive developmental series are available, the growth patterns from these basal and mostly simple morphologies and topologies can be easily reconstructed up to their fully-grown and sometimes highly diverged adult stage (Zeller 1983, 1989).

We revealed the terminology of intranasal morphologies to establish a primate-specific template for recording traits according to Sereno's (2007) phenotyping approach. A trait (i.e., a morphological structure) is either absent or present, and its expression is described based on qualitative (shape) or quantitative (e.g., size) data (Sereno 2007; Stefen et al. 2022). Our data strikingly revealed two challenges for the use of the phenotyping approach. First, phenotypic data ignores polymorphism (e.g., three and four ETs in the *Lemur* series) because it requires the assignment of one character state (i.e., three or four) to a trait (number of ETs). Second, different developmental origins might indicate that although turbinals share a similar topology in adults, they may be not necessarily homologous (in our present example ET "III" in platyrrhines to ET III in strepsirrhines and non-primate placentals). Both findings may bias the analyses of phenotypic data like their alignment with genotypes or their use in phylogenetic analyses. The application of phenotyping still requires its user to take a close look at the primary (i.e., descriptive, text-based) data, too, in order to entirely unravel possible contrary results. For instance, we strongly suggest that ET III has become lost independently in catarrhines and platyrrhines (Lundeen and Kay 2022), and that a convergent turbinal has evolved in some platyrrhine lineages as an apomorphic trait (Fig. 9). However, this may apply to the osseous turbinals; we cannot extend the argument to turbinals as mucosal folds. The early, likely programmed outgrowth of the turbinal as a soft tissue structure may well still be homologous.

Conclusions

The primary aim of the current study was the identification of intranasal structures—the individual turbinals in particular—across a limited sample of primates based on comparative ontogenetic series. The exact identification of homologous morphological structures is a prerequisite for linking phenotypes to other data like genotypes (e.g., Prudent et al. 2016; Zoonomia Project, Christmas et al. 2023), and plotting traits on phylogenetic trees (Stößel et al. 2010; Christmas et al. 2023). Otherwise, such analyses may incorrectly estimate character states for ancestral nodes. We revealed three key features that challenge assumptions about homology. First, across the age series we observed varying growth patterns of several structures. Turbinals which seem to be homologous between species in adult specimens exhibit in fact different ontogenetic origins (ET III in strepsirrhines vs. ET "III" in *Aotus* and *Pithecia*). These heterochronic patterns need to be considered when depending on the homology of traits. Second, based on our sample we cannot yet infer the homology of the FTs in strepsirrhines; and accordingly followed the simple count from medial to lateral/ventral (Smith and Rossie 2008). Third, we found evidence that the number of ETs and FTs may not be species-specific as previously suggested (Ruf 2014; Wagner and Ruf 2021). Whether variations in some placental species are common, or the microsmatic haplorhines are just consistent with Darwin's (1859) observation that traits which are not subjected to selective pressure vary, needs to be evaluated on larger samples.

Our study used a limited species sample. Future studies should expand the number of species, and consider other phenotypic traits beside the turbinal number like morphometric data (e.g., surface area), geometric morphometrics (e.g., topology), and physiology (e.g., distribution and thickness of olfactory epithelium). These traits are considered to be more associated with the number of OR genes, and to represent more reliable proxies to infer olfactory performance (Smith et al. 2004; Yohe et al. 2022; Martinez et al. 2023). When referring to grundplan reconstruction, fossil species need to be included into phylogenetic analyses as they provide basic information about plesiomorphic traits (Lundeen and Kirk 2019; Kirk and Lundeen 2020; Lundeen and Kay 2022).

Acknowledgements

We are grateful to V. Rosenberger (SRU) who stained some histological sections; C. Vinyard (Ohio University) provided µCT scans of several specimens. Creation of datasets accessed on MorphoSource (https://www.morphosource.org) was made possible by the following funders and grant numbers: NSF DDIG #0925793 and the Wenner Gren Foundation (Media ID 000003030, Media ID 000003052), and the AMNH and NYCEP (Media ID 000016131). We also thank R. Bryson and K. Franklin (UF) for support in the application of 3D Slicer. The project is funded by the Walter Benjamin Fellowship of the Deutsche Forschungsgemeinschaft (Project # 507060877), by the National Science Foundation (grant #s BCS-2235657, BCS-2235578, BCS-1830919, and BCS-1830894), and in part by the Emory National Primate Research Center (Grant No. ORIP/OD P51OD011132). We would also thank our reviewers T. Macrini and Q. Martinez for their suggestions to improve our manuscript. This is DLC publication # 1596.

References

Allen H (1882) On a revision of the ethmoid bone in the Mammalia. Bulletin of the Museum of Comparative Zoology 10: 135164.

Bonnet R (1897) Beiträge zur Embryologie des Hundes. Anatomische Hefte 9: 419–512.

Cabej NR (2012) Ontogeny: The workshop of evolutionary change. In: Cabej NR (Ed.) Epigenetic Principles of Evolution. Elsevier, Amsterdam, 307–326. https://doi.org/10.1016/B978-0-12-415831-3.00009-4

Christmas MJ, Kaplow IM, Genereux DP, Dong MX, Graham M. Hughes GM, Li X, Sullivan PF, Hindle AG, Andrews G, Armstrong JC, Bianchi M, Breit AM, Diekhans M, Fanter C, Foley NM, Goodman DB, Goodman L, Keough KC, Kirilenko B, Kowalczyk A, Lawless C, Lind AL, Meadows JRS, Moreira LR, Redlich RW, Ryan L, Swofford R, Valenzuela A, Wagner F, Wallerman O, Brown AR, Damas J, Fan K, Gatesy J, Grimshaw J, Johnson J, Kozyrev SV, Lawler AJ, Marinescu VD, Morrill KM, Osmanski A, Paulat NS, Phan BDN, Reilly SK, Schäffer DE, Steiner C, Supple MA, Wilder AP, Wirthlin ME, Xue JR, Birren BW, Gazal S, Hubley RM, Koepfli K-P, Marques-Bonet T, Meyer WK, Nweeia M, Sabeti PC, Shapiro B, Smit AFA, Springer MS, Teeling EC, Weng Z, Hiller M, Levesque DL, Lewin HA, Murphy WJ, Navarro A, Paten B, Pollard KS, Ray DA, Ruf I, Ryder OA, Pfenning AR, Lindblad-Toh K, Karlsson EK (2023) Evolutionary constraint and innovation across hundreds of placental mammals. Science 380: eabn3943. https://doi.org/10.1126/science.abn3943

Darwin C (1859) On the Origin of Species by Means of Natural Selection, or the Preservation of Favoured Races in the Struggle for Life. John Murray, London, 502 pp.

DeLeon VB, Franklin KP, Haynes LK, Vinyard CJ, Smith TD (2022) Ectochondral bone: The role of membranes in shaping endochondral bones of the skull. American Journal of Biological Anthropology 177, S73, Program of the 91st Annual Meeting of the American Association of Biological Anthropologists: 44–45. https://doi.org/10.1002/ajpa.24514open_in_new

DeLeon VB, Smith TD (2014) Mapping the nasal airways: Using histology to enhance CT-based three-dimensional reconstruction in *Nycticebus*. Anatomical Record 297: 2113–2120. https://doi.org/10.1002/ar.23028

Evans N, Krajian A (1930) New method of decalcification. Archives of Pathology 10: 447.

Fedorov A, Beichel R, Kalpathy-Cramer J, Finet J, Fillion-Robin J-C, Pujol S, Bauer C, Jennings D, Fennessy FM, Sonka M, Buatti J, Aylward SR, Miller JV, Pieper S, Kikinis R (2012) 3D Slicer as an Image Computing Platform for the Quantitative Imaging Network. Magnetic Resonance Imaging 30: 1323–1341. https://doi.org/10.1016/j.mri.2012.05.001

Genereux DP, Serres A, Armstrong J, Johnson J, Marinescu VD, Murén E, Juan D, Bejerano G, Casewell NR, Chemnick LG, Damas J, Di Palma F, Diekhans M, Fiddes IT, Garber M, Gladyshev VN, Goodman L, Haerty W, Houck ML, Hubley R, Kivioja T, Koepfli K-P, Kuderna LFK, Lander ES, Meadows JRS, Murphy WJ, Nash W, Noh HJ, Nweeia M, Pfenning A, Pollard KS, Ray DA, Shapiro B, Smit AFA, Springer MS, Steiner CC, Swofford R, Taipale J, Teeling EC, Turner-Maier J, Alfoldi J, Birren B, Ryder OA, Lewin HA, Paten B, Marques-Bonet T, Lindblad-Toh K, Karlsson EK (2020) A comparative genomics multitool for scientific discovery and conservation. Nature 587: 240–245. https://doi.org/10.1038/s41586-020-2876-6

Gill GW, Frost JK, Miller KA (1974) A new formula for half-oxidised hematoxylin solution that neither overstains or requires differentiation. Acta Cytologica 18: 300–311.

Gomori G (1950) A rapid one-step trichrome stain. American Journal of Clinical Pathology 20: 661–664. https://doi.org/10.1093/ajcp/20.7_ts.661

Harvey PH, Clutton-Brock TH (1985) Life history variation in primates. Evolution 39: 559–581. https://doi.org/10.1111/j.1558-5646.1985.tb00395.x

Haszprunar G (1998) Parsimony analysis as a specific kind of homology estimation and the implications for character weighting. Molecular Phylogenetics and Evolution 9: 333–339. https://doi.org/10.1006/mpev.1998.0496

Hautier L, Gomes Rodrigues H, Billet G, Asher RJ (2016) The hidden teeth of sloths: Evolutionary vestiges and the development of a simplified dentition. Scientific Reports 6: 27763. https://doi.org/10.1038/srep27763

Ito K, Kodeara R, Koyasu K, Martinez Q, Koyabu D (2022) The development of nasal turbinal morphology of moles and shrews. Vertebrate Zoology 72: 857–881. https://doi.org/10.3897/vz.72.e85466

Ito K, Tu VT, Eiting TP, Nojiri T, Koyabu D (2021) On the embryonic development of the nasal turbinals and their homology in bats. Frontiers in Cell and Developmental Biology 9: 613545. https://doi.org/10.3389/fcell.2021.613545

Kavanagh KD, Bailey CS, Sears KE (2020) Evidence of five digits in embryonic horses and developmental stabilization of tetrapod digit number. Proceedings of the Royal Society B 287: 20192756. https://doi.org/10.1098/rspb.2019.2756

Kirk EC, Lundeen IK (2020) New observations of the nasal fossa and interorbital region of *Shoshonius cooperi* based on microcomputerized tomography. Journal of Human Evolution 141: 102748. https://doi.org/10.1016/j.jhevol.2020.102748

Lundeen IK, Kay RF (2022) Unique nasal turbinal morphology reveals *Homunculus patagonicus* functionally converged on modern platyrrhine olfactory sensitivity. Journal of Human Evolution 167: 103184. https://doi.org/10.1016/j.jhevol.2022.103184

Lundeen IK, Kirk EC (2019) Internal nasal morphology of the Eocene primate *Rooneyia viejaensis* and extant Euarchonta: Using µCT scan data to understand and infer patterns of nasal fossa evolution in primates. Journal of Human Evolution 132: 137–173. https://doi.org/10.1016/j.jhevol.2019.04.009

Macrini TE (2012) Comparative morphology of the internal nasal skeleton of adult marsupials based on X-ray computed tomography. Bulletin of the American Museum of Natural History 365: 1–91. http://www.bioone.org/doi/full/10.1206/365.1

Macrini TE (2014) Development of the ethmoid in *Caluromys philander* (Didelphidae, Marsupialia) with a discussion on the homology of the turbinal elements in marsupials. Anatomical Record 297: 2007–2017. https://doi.org/10.1002/ar.23024

Macrini TE, Hopwood J, Herbert CA, Weisbecker V (2023) Development of the ethmoid in a wallaby and implications for the homology of turbinal elements in marsupials. Philosophical Transactions of the Royal Society B 378: 20220082. https://doi.org/10.1098/rstb.2022.0082

Maier W (1980) Nasal structures in Old and New World primates. In: Ciochon RL, Chiarelli AB (Eds) Evolutionary Biology of the New World Monkeys and Continental Drift. Plenum Press, New York, NY, 219–241.

Maier W (1993a) Cranial morphology of the therian common ancestor, as suggested by the adaptations of neonate marsupials. In: Szalay F, Novacek M, McKenna M (Eds) Mammal Phylogeny. Springer, New York, NY, 165–181. https://doi.org/10.1007/978-1-4613-92-49-1_12

Maier W (1993b) Zur evolutiven und funktionellen Morphologie des Gesichtsschädels der Primaten. Zeitschrift für Morphologie und Anthropologie 79: 279–299. https://www.jstor.org/stable/25757386

Maier W (2000) Ontogeny of the nasal capsule in cercopithecoids: A contribution to the comparative and evolutionary morphology of catarrhines. In: Whitehead PF, Jolly CJ (Eds) Old World Monkeys. Cambridge University Press, Cambridge, 99–132. https://doi.org/10.1017/CBO9780511542589.006

Maier W, Ruf I (2014) Morphology of the nasal capsule of primates—with special reference to *Daubentonia* and *Homo*. Anatomical Record 297: 1985–2006. https://doi.org/10.1002/ar.23023

Martinez Q, Amson E, Laska M (2024a) Does the number of functional olfactory receptor genes predict olfactory sensitivity and discrimination performance in mammals? Journal of Evolutionary Biology 37: 238–247. https://doi.org/10.1093/jeb/voae006

Martinez Q, Amson E, Ruf I, Smith TD, Pirot N, Broyon M, Lebrun R, Captier G, Martín CG, Ferreira GS, Fabre P-H (2024b) Turbinal bones are still one of the last frontiers of the tetrapod skull: Hypotheses, challenges and perspectives. PaleorXiv. https://doi.org/10.31233/osf.io/2gm95

Martinez Q, Courcelle M, Douzery E, Fabre P-H (2023) When morphology does not fit the genomes: The case of rodent olfaction. Biology Letters 19: 20230080. https://doi.org/10.1098/rsbl.2023.0080

McCune AR, Schimenti JC (2012) Using genetic networks and homology to understand the evolution of phenotypic traits. Current Genomics 13: 74–84. https://dx.doi.org/10.2174/138920212799034785

Melin AD, Fedigan LM, Hiramatsu C, Hiwatashi T, Parr N, Kawamura S (2009) Fig foraging by dichromatic and trichromatic *Cebus capucinus* in a tropical dry forest. International Journal of Primatology 30: 753–775. https://doi.org/10.1007/s10764-009-9383-9

Paulli S (1900a) Über die Pneumaticität des Schädels bei den Säugetieren. Eine morphologische Studie. I. Über den Bau des Siebbeins. Über die Morphologie des Siebbeins und die Pneumaticität bei den Monotremen und den Marsupialiern. Morphologisches Jahrbuch 28: 147–178.

Paulli S (1900b) Über die Pneumaticität des Schädels bei den Säugetieren. Eine morphologische Studie. II. Über die Morphologie des Siebbeins und der Pneumaticität bei den Ungulaten und Proboscicden. Morphologisches Jahrbuch 28: 179–251.

Paulli S (1900c) Über die Pneumaticität des Schädels bei den Säugetieren. Eine morphologische Studie. III. Über die Morphologie des Siebbeins und die Pneumaticität bei den Insectivoren, Hyracoideen, Chiropteren, Carnivoren, Pinnipeden, Edentaten, Rodentiern, Prosimiern und Primaten, nebst einer zusammenfassenden Übersicht über die Morphologie des Siebbeins und die der Pneumaticität des Schädels bei den Säugetieren. Morphologisches Jahrbuch 28: 483–564.

Prudent X, Parra G, Schwede P, Roscito JG, Hiller M (2016) Controlling for phylogenetic relatedness and evolutionary rates improves the discovery of associations between species' phenotypic and genomic differences. Molecular Biology and Evolution 33: 2135–2150. https://doi.org/10.1093/molbev/msw098

Reinbach W (1952a) Zur Entwicklung des Primordialcraniums von *Dasypus novemcinctus* Linné (*Tatusia novemcinctus* Lesson) I. Zeitschrift für Morphologie und Anthropologie 44: 375–444. https://www.jstor.org/stable/25753216

Reinbach W (1952b) Zur Entwicklung des Primordialcraniums von *Dasypus novemcinctus* Linné (*Tatusia novemcinctus* Lesson) II. Zeitschrift für Morphologie und Anthropologie 45: 1–72. https://www.jstor.org/stable/25753226

Ross CF (1995) Allometric and functional influences on primate orbit orientation and the origins of the Anthropoidea. Journal of Human Evolution 29: 201–227. https://doi.org/10.1006/jhev.1995.1057

Ruf I (2014) Comparative anatomy and systematic implications of the turbinal skeleton in Lagomorpha (Mammalia). Anatomical Record 297: 2031–2046. https://doi.org/10.1002/ar.23027

Rylands AB, Heymann EW, Lynch Alfaro J, Buckner JC, Roos C, Matauschek C, Boubli JP, Sampaio R, Mittermeier RA (2016) Taxonomic review of the New World tamarins (Primates: Callitrichidae). Zoological Journal of the Linnean Society 177: 1003–1028. https://doi.org/10.1111/zoj.12386

Sánchez-Villagra MR, Forasiepi AM (2017) On the development of the chondrocranium and the histological anatomy of the head in perinatal stages of marsupial mammals. Zoological Letters 3: 1–33. https://doi.org/10.1186/s40851-017-0062-y

Schrenk F (1989) Zur Schädelentwicklung von *Ctenodactylus gundi* (Rothmann 1776) (Mammalia: Rodentia). Courier Forschungsinstitut Senckenberg 108: 1–241.

Semon R (1894) Zur Entwickelungsgeschichte der Monotremen. Denkschriften der Medicinisch-Naturwissenschaftlichen Gesellschaft zu Jena 5: 61–74.

Sereno PC (2007) Logical basis for morphological characters in phylogenetics. Cladistics 23: 565–587. https://doi.org/10.1111/j.1096-0031.2007.00161.x

Seydel O (1891) Ueber die Nasenhöhle der höheren Säugethiere und des Menschen. Morphologisches Jahrbuch 17: 44–99.

Smith TD, Bhatnagar KP (2004) Microsmatic primates: Reconsidering how and when size matters. Anatomical Record 279B: 24–31. https://doi.org/10.1002/ar.b.20026

Smith TD, Bhatnagar KP, Rossie JB, Docherty BA, Burrows AM, Cooper GM, Mooney MP, Siegel MI (2007) Scaling the first ethmoturbinal in nocturnal strepsirrhines: Olfactory and respiratory surfaces. Anatomical Record 290: 215–237. https://doi.org/10.1002/ar.20428

Smith TD, Bhatnagar KP, Tuladhar P, Burrows AM (2004) Distribution of olfactory epithelium in the primate nasal cavity: Are microsmia and macrosmia valid morphological concepts? Anatomical Record 281A: 1173–1181. https://doi.org/10.1002/ar.a.20122

Smith TD, Craven BA, Engel SM, Bonar CJ, DeLeon VB (2019) Nasal airflow in the pygmy slow loris (*Nycticebus pygmaeus*) based on a combined histological, computed tomographic and computational fluid dynamics methodology. Journal of Experimental Biology 222: jeb207605. https://doi.org/10.1242/jeb.207605

Smith TD, Curtis A, Bhatnagar KP, Santana SE (2021a) Fissures, folds, and scrolls: The ontogenetic basis for complexity of the nasal cavity in a fruit bat (*Rousettus leschenaultii*). Anatomical Record 304: 883–900. https://doi.org/10.1002/ar.24488

Smith TD, DeLeon VB, Vinyard CJ, Young, JW (2020) Skeletal Anatomy of the Newborn Primate. Cambridge University Press, Cambridge, 307 pp. https://doi.org/10.1017/9781316591383

Smith TD, Kentzel ES, Cunningham JM, Bruening AE, Jankord KD, Trupp SJ, Bonar C, Rehorek SJ, DeLeon VB (2014a) Mapping bone cell distributions to assess ontogenetic origin of primate midfacial form. American Journal of Physical Anthropology 154: 424–435. https://doi.org/10.1002/ajpa.22540

Smith TD, Laitman JT, Bhatnagar KP (2014b) The shrinking anthropoid nose, the human vomeronasal organ, and the language of anatomical reduction. Anatomical Record 297: 2196–2204. https://doi.org/10.1002/ar.23035

Smith TD, Martell MC, Rossie JB, Bonar CJ, DeLeon VB (2016) Ontogeny and microanatomy of the nasal turbinals in Lemuriformes. Anatomical Record 299: 1492–1510. https://doi.org/10.1002/ar.23465

Smith TD, McMahon MJ, Millen ME, Llera C, Engel SM, Li L, Bhatnagar KP, Burrows AM, Zumpano MP, DeLeon VB (2017) Growth and development at the sphenoethmoidal junction in perinatal primates. Anatomical Record 300: 2115–2137. https://doi.org/10.1002/ar.23630

Smith TD, Muchlinski MN, Jankord KD, Progar AJ, Bonar CJ, Evans S, Williams L, Vinyard CJ, DeLeon VB (2015) Dental maturation, eruption, and gingival emergence in the upper jaw of newborn primates. Anatomical Record 298: 2098–2131. https://doi.org/10.1002/ar.23273

Smith TD, Rossie JB (2006) Primate olfaction: Anatomy and evolution. In: Brewer WJ, Castle D, Pantelis C (Eds) Olfaction and the Brain. Cambridge University Press, Cambridge, 135–166. https://doi.org/10.1017/CBO9780511543623.010

Smith TD, Rossie JB (2008) Nasal fossa of mouse and dwarf lemurs (Primates, Cheirogaleidae). Anatomical Record 291: 895–915. https://doi.org/10.1002/ar.20724

Smith TD, Rossie JB, Docherty BA, Cooper GM, Bonar CJ, Silverio AL, Burrows AM (2008) Fate of the nasal capsular cartilages in prenatal and perinatal tamarins (*Saguinus geoffroyi*) and extent of secondary pneumatization of maxillary and frontal sinuses. Anatomical Record 291: 1397–1413. https://doi.org/10.1002/ar.20787

Smith TD, Siegel MI, Bonar CJ, Bhatnagar KP, Mooney MP, Burrows AM, Smith MA, Maico LM (2001) The existence of the vomeronasal organ in postnatal chimpanzees and evidence for its homology with that of humans. Journal of Anatomy 198: 77–82. https://doi.org/10.1046/j.1469-7580.2001.19810077.x

Smith TD, Ufelle AC, Cray JJ, Rehorek SB, DeLeon VB (2021b) Inward collapse of the nasal cavity: Perinatal consolidation of the midface and cranial base in primates. Anatomical Record 304: 939–957. https://doi.org/10.1002/ar.24537

Smith TD, Zinreich SJ, Márquez S, King SE, Evans S, DeLeon VB (2023) Growth and microanatomy of the paranasal sinuses in two species of New World monkeys. Anatomical Record 307: 49–65. https://doi.org/10.1002/ar.25222

Smuts B, Nicolson N (1989) Reproduction in wild female olive baboons. American Journal of Primatology 19: 229–246. https://doi.org/10.1002/ajp.1350190405

Stefen C, Wagner F, Asztalos M, Giere P, Grobe P, Hiller M, Hofmann R, Jähde M, Lächele U, Lehmann T, Ortmann S, Peters B, Ruf I, Schiffman C, Thier N, Unterhitzenberger G, Vogt L, Rudolf M, Wehner P, Stuckas H (2022) Phenotyping in the era of genomics: *MaTrics*—a digital character matrix to document mammalian phenotypic traits. Mammalian Biology 102: 235–249. https://doi.org/10.1007/s42991-021-00192-5

Stößel A, Junold A, Fischer MS (2010) The morphology of the eutherian ethmoidal region and its implications for higher-order phylogeny. Journal of Zoological Systematics and Evolutionary Research 48: 167–180. https://doi.org/10.1111/j.1439-0469.2009.00560.x

Swindler DR (2002) Primate dentition: An introduction to the teeth of non-human primates. Vol. 32. Cambridge University Press, Cambridge, xvi, 296 pp. https://doi.org/10.1017/CBO9780511542541

Urbani B (2002) A field observation on color selection by New World sympatric primates, *Pithecia pithecia* and *Alouatta seniculus*. Primates 43: 95–101. https://doi.org/10.1007/BF02629669

Van Valkenburgh B, Smith TD, Craven BA (2014) Tour of a labyrinth: Exploring the vertebrate nose. Anatomical Record 297: 1975–1984. https://doi.org/10.1002/ar.23021

Voit M (1909) Das Primordialcranium des Kaninchens unter Berücksichtigung der Deckknochen. Ein Beitrag zur Morphologie des Säugetierschädels. Anatomische Hefte 38: 425–616.

Wagner F, Ruf I (2019) Who nose the borzoi? Turbinal skeleton in a dolichocephalic dog breed (*Canis lupus familiaris*). Mammalian Biology 94: 106–119. https://doi.org/10.1016/j.mambio.2018.06.005

Wagner F, Ruf I (2021) "Forever young"—Postnatal growth inhibition of the turbinal skeleton in brachycephalic dog breeds (*Canis lupus familiaris*). Anatomical Record 304: 154–189. https://doi.org/10.1002/ar.24422

Werneburg I, Yaryhin O (2018) Character definition and tempus optimum in comparative chondrocranial research. Acta Zoologica 100: 376–388. https://doi.org/10.1111/azo.12260

Werneburg I, Tzika AC, Hautier L, Asher R, Milinkovitch MC, Sánchez-Villagra MR (2013) Development and embryonic staging in non-model organisms: The case of an afrotherian mammal. Journal of Anatomy 222: 2–18. https://doi.org/10.1111/j.1469-7580.2012.01509.x

Wood B, Oladipupo L, Mano N, Taylor J, Vinyard CJ, Cray J, DeLeon VB, Smith TD (2023) Midline growth of the sphenoid bone in primates: A histological and microcomputed tomography study. Anatomical Record 180: 127–143. https://doi.org/10.1002/ajpa.24653

Yohe LR, Fabbri M, Lee D, Davies KTJ, Yohe TP, Sánchez MKR, Rengifo EM, Hall RP, Mutumi G, Hedrick BP, Sadier A, Simmons NB, Sears KE, Dumont E, Rossiter SJ, Bhullar B-AS, Dávalos LM (2022) Ecological constraints on highly evolvable olfactory receptor genes and morphology in neotropical bats. Evolution 76: 2347–2360. https://doi.org/10.1111/evo.14591

Zeller U (1983) Zur Ontogenese und Morphogenese des Craniums von *Tupaia belangeri* (Tupaiidae, Scandentia, Mammalia). PhD Thesis, Universität Göttingen, Göttingen, Germany.

Zeller U (1989) Die Entwicklung und Morphologie des Schädels von *Ornithorhynchus anatinus* (Mammalia: Prototheria: Monotremata). Abhandlungen der Senckenbergischen Naturforschenden Gesellschaft 545: 1–188.

Zoonomia Consortium. https://zoonomiaproject.org

Supplementary Material 1

Tables S1–S16

Authors: Wagner F, DeLeon VB, Bonar CJ, Smith TD (2024)
Data type: .zip
Explanation notes: **Table S1.** µCT scan of the ethmoidal region of an early infant *Lemur catta* (DLC 6938f). — **Table S2.** µCT scan of the ethmoidal region of a juvenile *Lemur catta* (LCD 100121). — **Table S3.** Histological serial sections of the ethmoidal region in *Otolemur crassicaudatus* in coronal view (rostral to caudal). — **Table S4.** µCT scan of the ethmoidal region of an infant Otolemur crassicaudatus (DLC 2728).— **Table S5.** µCT scan of the turbinal skeleton in an adult *Otolemur garnettii* (CMNH B0748). — **Table S6.** µCT scans of the ethmoidal region of an adult *Saguinus imperator* (M60903).— **Table S7.** 14 days-old infant *Aotus nancymaae* (Aotus104), revealing the histological composition of the third ethmoturbinal (ET III). — **Table S8.** µCT scan of the ethmoidal region in an adult *Aotus nancymaae* (Aotus1). — **Table S9.** Nasal cavity of two *Pithecia pithecia neonates*: histological sections of Saki2, diceCT scan of Saki3. — **Table S10.** µCT scan of the ethmoidal region of an adult *Pithecia pithecia* (CMNH-11-F3). — **Table S11.** Ethmoidal region in a mid-fetal macaque (*Macaca fascicularis*, CRL 55 mm); schematic illustration redrawn after Maier (2000, fig. 5.2: serial sections # 14-3-2, 20-2-2). — **Table S12.** µCT scan of the ethmoidal region of a subadult *Macaca nemestrina* (516-A6). — **Table S13.** µCT scans of the ethmoidal region in three *Macaca* species: *M. fascicularis* (adult, mcz:mamm:23812*); *M. mulatta* (adult, MCZ:Mamm:26475**); *M. nemestrina* (adolescent, A3). */** Datasets accessed on MorphoSource (https://www.morphosource.org, *Media ID 000003030, **Media ID 000003052). — **Table S14.** µCT scan of the ethmoidal region in an adult *Papio anubis* (amnh:mammals:m-51380). Dataset accessed on MorphoSource (https://www.morphosource.org, Media ID 000016131). — **Table S15.** Developmental states in the turbinal skeleton across the age stages in two strepsirrhines, *Lemur catta* and *Otolemur* spp.— **Table S16.** Developmental states in the turbinal skeleton across the age stages in haplorhines.

Link: https://doi.org/10.3897/vz.74.e126944.suppl1